Inverse Problems **26** (2010) 025008 (27pp) doi:10.1088/0266-5611/26/2/025008

Synthetic-aperture radar imaging through dispersive media

Trond Varslot[1], **J Héctor Morales**[2] **and Margaret Cheney**[3]

[1] Department of Applied Mathematics, Australian National University, Acton, 0200 ACT, Australia
[2] Centro de Investigación en Matemáticas, A. C. Jalisco S/N, Col. Valenciana, 36240 Guanajuato, Gto, Mexico
[3] Department of Mathematical Sciences, Rensselaer Polytechnic Institute, Troy, NY 12180-3590, USA

E-mail: trond@varslot.net, moralesjh@cimat.mx and cheney@rpi.edu

Received 17 June 2009, in final form 9 December 2009
Published 12 January 2010
Online at stacks.iop.org/IP/26/025008

Abstract

In this paper we develop a method for synthetic-aperture radar (SAR) imaging through a dispersive medium. We consider the case when the sensor and scatterers are embedded in a known homogeneous dispersive material, the scene to be imaged lies on a known surface and the radar antenna flight path is an arbitrary but known smooth curve. The scattering is modeled using a linearized (Born) scalar model. We assume that the measurements are polluted with additive noise. Furthermore, we assume that we have prior knowledge about the power-spectral densities of the scene and the noise. This leads us to formulate the problem in a statistical framework. We develop a filtered-back-projection imaging algorithm in which we choose the filter according to the statistical properties of the scene and noise. We present numerical simulations for a case where the scene consists of point-like scatterers located on the ground, and demonstrate how the ability to resolve the targets depends on a quantity which we call the *noise-to-target ratio*. In our simulations, the dispersive material is modeled with the Fung–Ulaby equations for leafy vegetation. However, the method is also applicable to other dielectric materials where the dispersion is considered relevant in the frequency range of the transmitted signals.

1. Introduction

If the speed of wave propagation in a medium depends on frequency, the medium is said to be *dispersive*. All materials are dispersive to some extent [1]; however, almost all current work on radar imaging neglects the effect of dispersion. For most radar systems, this is a reasonable assumption because (a) the dispersion is very weak in dry air and (b) the frequency bands of

most radar systems are not wide enough for dispersive effects to be important. However, it is well known that range resolution is proportional to the bandwidth. As a consequence, high-resolution systems require broadband pulses for which the issue of dispersion may become important. Therefore, it is of interest to develop synthetic-aperture radar (SAR) imaging algorithms that account for dispersive wave propagation [2, 3].

SAR image formation is closely related to the solution of an inverse scattering problem. The time-domain direct and inverse scattering problems for dispersive media have been extensively studied by many authors [4–10]. However, most of this work is for the one-dimensional case. An optimization-based reconstruction of a parametrized multidimensional dispersive medium was demonstrated in [11]. The analysis of the effect of propagation through the dispersive ionosphere on SAR image formation was recently carried out in [12]. A method for performing SAR imaging through a weakly dispersive layer was developed in [2], where the wave propagation was modeled in terms of a Fourier integral operator (FIO).

In this paper we will develop an algorithm for forming SAR images of objects that are embedded in a known homogeneous dispersive background. This paper is mainly based on SAR imaging methods as formulated in [13] and [14] for non-dispersive media, and complements the statistical approach developed in [15] and [16] for dealing with measurements that are corrupted by noise. Although we follow the general strategy of [2], we find that our linearized forward model is not a FIO, and thus our imaging algorithm does not follow from the FIO theory.

This paper is divided into five sections. In section 2 we provide the mathematical model for scattering in a dispersive medium. We proceed to derive the filtered-back-projection method in section 3, where the main result is stated as theorem 3.2. Numerical examples in section 4 illustrate the implementation of the algorithm. Some concluding remarks are given in section 5.

2. Wave propagation through a dispersive medium

We consider the case in which the region between the sensors and the scattering objects ('targets') consists of a known, homogeneous, dispersive medium ('atmosphere').

In this section we give a brief review of the wave equations that govern the evolution of electromagnetic fields in the presence of scatterers in a dispersive medium.

2.1. Maxwell's equations and constitutive relations

Our starting point is the Maxwell equations, which are given in differential form by [17]

$$\nabla \cdot \boldsymbol{D}(\mathbf{x}, t) = \rho(\mathbf{x}, t) \tag{1a}$$

$$\nabla \cdot \boldsymbol{B}(\mathbf{x}, t) = 0 \tag{1b}$$

$$\nabla \times \boldsymbol{E}(\mathbf{x}, t) = -\partial_t \boldsymbol{B}(\mathbf{x}, t) \tag{1c}$$

$$\nabla \times \boldsymbol{H}(\mathbf{x}, t) = \partial_t \boldsymbol{D}(\mathbf{x}, t) + \boldsymbol{J}(\mathbf{x}, t). \tag{1d}$$

Here, $\boldsymbol{D}$ is the electric displacement, $\boldsymbol{B}$ is the magnetic induction, $\boldsymbol{E}$ is the electric field, $\boldsymbol{H}$ is the magnetic field, ρ is the charge density and $\boldsymbol{J}$ is the current density. The variable $\mathbf{x} = (x_1, x_2, x_3)^{\mathrm{T}} \in \mathbb{R}^3$ represents Cartesian coordinates and $t \in \mathbb{R}$ is time. Finally, $\nabla \cdot$ denotes the divergence operator and $\nabla \times$ denotes the curl operator.

In order to complete this set of equations, we need to add some constitutive relations. We will use the following relations [4, 18]:

$$\boldsymbol{D}(\mathbf{x}, t) = \int_0^\infty \varepsilon(\mathbf{x}, t')\boldsymbol{E}(\mathbf{x}, t - t')\,\mathrm{d}t' := (\varepsilon \underset{t}{*} \boldsymbol{E})(\mathbf{x}, t), \tag{2a}$$

$$\boldsymbol{B}(\mathbf{x}, t) = \mu_0 \boldsymbol{H}(\mathbf{x}, t). \tag{2b}$$

Here μ_0 denotes the free-space magnetic permeability. We should note that since $\varepsilon(\mathbf{x}, t) := 0$ for $t < 0$, we are guaranteed that the constitutive relation obeys causality; the dielectric response of the medium will be affected by the applied field $\boldsymbol{E}$ only at earlier times.

We will frequently write quantities in the temporal frequency domain. As an example, we can express the electric field, $\boldsymbol{E}$, in terms of its Fourier transform, $\tilde{\boldsymbol{E}}(\mathbf{x}, \omega)$, as

$$\boldsymbol{E}(\mathbf{x}, t) = \frac{1}{2\pi} \int \mathrm{e}^{-\mathrm{i}\omega t} \tilde{\boldsymbol{E}}(\mathbf{x}, \omega)\,\mathrm{d}\omega, \tag{3}$$

The frequency-domain counterpart of the dielectric constitutive relation in (2*a*) is given by

$$\tilde{\boldsymbol{D}}(\mathbf{x}, \omega) = \epsilon(\mathbf{x}, \omega)\tilde{\boldsymbol{E}}(\mathbf{x}, \omega). \tag{4}$$

Here $\epsilon(\mathbf{x}, \omega)$ is the Fourier transform of $\varepsilon(\mathbf{x}, t)$.

2.2. Dispersion, wave numbers and index of refraction

For a dispersive medium, the permittivity ϵ not only is frequency dependent, but also, in order to obey the causality requirement in our constitutive relation, must be complex-valued. In terms of the relative permittivity of the medium $\epsilon_r = \epsilon/\epsilon_0$, the *index of refraction* is

$$n(\omega) := \sqrt{\epsilon_r(\omega)}, \tag{5}$$

and is therefore also a complex-valued function; we denote the real and imaginary parts of n by n_R and n_I, respectively:

$$n(\omega) := n_R(\omega) + \mathrm{i}\, n_I(\omega). \tag{6}$$

In order to avoid unphysical solutions, we choose the branch of the square root in (5) such that $\omega n_I(\omega)$ has positive sign. This branch corresponds to attenuation rather than amplification of the propagating electromagnetic waves. See section 1.3 in [19] for a detailed discussion of the index of refraction.

The *phase velocity* v_p is the speed at which the phase of any one frequency component propagates. It is

$$v_p(\omega) := \frac{c_0}{n_R(\omega)}. \tag{7}$$

Here $c_0 = 1/\sqrt{\mu_0\epsilon_0}$ is the speed of light in vacuum.

We will also use the (complex) *wave number* $k(\omega) := \omega n(\omega)/c_0 = \omega\sqrt{\epsilon_r(\omega)}/c_0$.

2.3. The scalar wave model

To arrive at the wave equation for the electric field in a homogeneous dispersive medium, we use equations (2*a*) and (2*b*) to eliminate $\boldsymbol{D}$ and $\boldsymbol{B}$ in (1*c*) and (1*d*). Then we substitute the curl of (1*c*) into (1*d*), and end up with

$$\nabla \times \nabla \times \boldsymbol{E} = -\partial_t \mu_0 \boldsymbol{J} - \partial_t^2(\mu_0 \varepsilon \underset{t}{*} \boldsymbol{E}). \tag{8}$$

We use the identity

$$\nabla \times \nabla \times \boldsymbol{E} = \nabla(\nabla \cdot \boldsymbol{E}) - \nabla^2 \boldsymbol{E} \tag{9}$$

to write (8) as

$$\nabla^2 \boldsymbol{E} - \partial_t^2(\mu_0 \varepsilon \underset{t}{*} \boldsymbol{E}) = \nabla(\nabla \cdot \boldsymbol{E}) + \mu_0 \partial_t \boldsymbol{J}. \tag{10}$$

We denote the right-hand side of (10) by $-\boldsymbol{J}_s$, which converts (10) into

$$\nabla^2 \boldsymbol{E} - \partial_t^2(\mu_0 \varepsilon \underset{t}{*} \boldsymbol{E}) = -\boldsymbol{J}_s. \tag{11}$$

In a homogeneous material with no sources, $\nabla \cdot \boldsymbol{E} = 0$ and $\boldsymbol{J} = 0$, which implies that the source term $\boldsymbol{J}_s$ is nonzero only where sources or scatterers are present. As a result, each component of the electric field satisfies a scalar wave equation of the form

$$\nabla^2 E - \partial_t^2\big(c_0^{-2} \varepsilon_r \underset{t}{*} E\big) = -j_s. \tag{12}$$

Here j_s denotes one component of $\boldsymbol{J}$ in (11).

2.4. Scattering model

In radar problems, the source $\boldsymbol{J}_s$ of (11) is a sum of two terms, $\boldsymbol{J}_s = \boldsymbol{J}^{\text{in}} + \boldsymbol{J}^{\text{sc}}$, where $\boldsymbol{J}^{\text{in}}$ models the transmitting antenna and $\boldsymbol{J}^{\text{sc}}$ models the scattering object [20]. The solution $\boldsymbol{E}$, which we write as $\boldsymbol{E}^{\text{tot}}$, therefore splits into two parts: $\boldsymbol{E}^{\text{tot}} = \boldsymbol{E}^{\text{in}} + \boldsymbol{E}^{\text{sc}}$. The first term, $\boldsymbol{E}^{\text{in}}$, satisfies the wave equation for the known, prescribed source $\boldsymbol{J}^{\text{in}}$. This part we call the *incident* field because it is incident upon the scatterers. The second term, $\boldsymbol{E}^{\text{sc}}$, is due to target scattering, and this part is called the *scattered* field. In our simplified scalar model, we write $E^{\text{tot}} = E^{\text{in}} + E^{\text{sc}}$, where E^{in} satisfies the wave equation for the known, prescribed source j_s^{in}.

In scattering problems, the source term $\boldsymbol{J}^{\text{sc}}$ (typically) represents the target's *response* to an incident field. This part of the source function will generally depend on the geometric and material properties of the target and on the form and strength of the incident field. Consequently, $\boldsymbol{J}^{\text{sc}}$ can be quite complicated to describe analytically, and in general it will not have the same direction as $\boldsymbol{J}^{\text{in}}$. Fortunately, for our purposes it is not necessary to provide a detailed analysis of the target's response; for stationary objects consisting of linear materials, we can write our scalar model j^{sc} as the time-domain convolution:

$$j^{\text{sc}}(t, \boldsymbol{x}) = \int v(t - t', \boldsymbol{x}) E^{\text{tot}}(t', \boldsymbol{x}) \, \mathrm{d}t', \tag{13}$$

where $v(t, \boldsymbol{x})$ is called the reflectivity function. In the full vector case, v would be a matrix operating on the full vector $\boldsymbol{E}^{\text{tot}}$; here we use only the single matrix element corresponding to the component considered in (12).

We make some assumptions about the nature of the background medium and about the scattering objects. These correspond to the situation shown in figure 1.

Assumption 2.1 (Scattering medium)**.** *We assume the following.*

(i) The background medium (atmosphere) is homogeneous with known relative permittivity $\varepsilon_r(t)$.

(ii) The complex part of the index of refraction, as defined in (6), tends to 0 for large ω *[19],* i.e.

$$\lim_{\omega \to \infty} n_I(\omega) = 0. \tag{14}$$

(iii) Electromagnetic scattering occurs at the surface given by

$$\mathbf{x} = \boldsymbol{\Psi}(x_1, x_2) := [x_1, x_2, \psi(x_1, x_2)]^{\mathrm{T}}, \tag{15}$$

where the function $\psi : \mathbb{R}^2 \mapsto \mathbb{R}$ *is assumed known.*

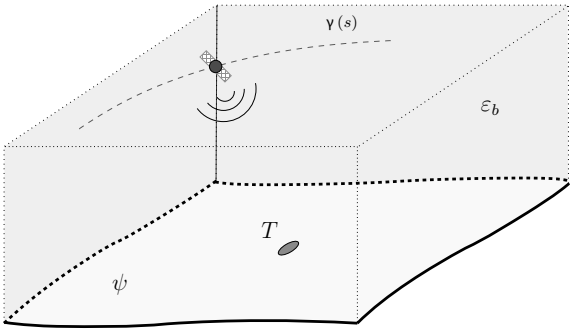

Figure 1. Background medium with a relative permittivity of ϵ_r, and a target which causes scattering due to a perturbation $c_0^2 T$ of the relative permittivity.

(iv) The target dispersion is known; in particular, when combined with (15) we assume that the reflectivity function can be written as $v(t, \boldsymbol{x}) = T(x_1, x_2)\delta(\mathbf{x} - \boldsymbol{\Psi}(x_1, x_2))\partial_t^2\delta(t)$.

We will use the term *target*, or *ground reflectivity function,* when we refer to T. The quantity T is what we want to reconstruct from measuring electromagnetic scattering (see figure 1).

2.4.1. The incident field. The incident field is the solution of the electric field which would have existed in the absence of the target. Therefore, the scalar version E^{in} will satisfy

$$\nabla^2 E^{\text{in}}(\mathbf{x}, t) - \partial_t^2\big(c_0^{-2}\varepsilon_r \underset{t}{*} E^{\text{in}}\big)(\mathbf{x}, t) = -j_s^{\text{in}}(\mathbf{x}, t). \tag{16}$$

In order to solve (16), we use the Green's function g that satisfies

$$\nabla^2 g(\mathbf{x}, \mathbf{y}, t) - \partial_t^2\big(c_0^{-2}\varepsilon_r \underset{t}{*} g\big)(\mathbf{x}, \mathbf{y}, t) = -\delta(\mathbf{x} - \mathbf{y})\delta(t), \tag{17}$$

together with the condition $g(\mathbf{x}, \mathbf{y}, t) = 0$ for $t < 0$. Here ε_r is the background permittivity from assumption 2.1. This Green's function represents the wavefield at $(\mathbf{x}, t)$ due to a point source at $\mathbf{y}$, at time $t = 0$.

To determine g, we take the temporal Fourier transform of (17), and obtain

$$(\nabla^2 + k^2(\omega))G(\mathbf{x}, \mathbf{y}, \omega) = -\delta(\mathbf{x} - \mathbf{y}), \tag{18}$$

where again $k(\omega) = \omega n(\omega)/c_0 = \omega\sqrt{\epsilon_r(\omega)}/c_0$, and ϵ_r and G denote the Fourier transform of ε_r and g, respectively. Equation (18) is solved by

$$G(\mathbf{x}, \mathbf{y}, \omega) = \frac{\mathrm{e}^{\mathrm{i}k(\omega)|\mathbf{x}-\mathbf{y}|}}{4\pi|\mathbf{x} - \mathbf{y}|}. \tag{19}$$

If we take the inverse Fourier transform of (19), we get a solution to (17):

$$g(\mathbf{x}, \mathbf{y}, t) = \frac{1}{8\pi^2}\int \frac{\mathrm{e}^{-\mathrm{i}\omega(t - n(\omega)|\mathbf{x}-\mathbf{y}|/c_0)}}{|\mathbf{x} - \mathbf{y}|}\,\mathrm{d}\omega. \tag{20}$$

For simplicity we consider an isotropic point-like antenna located at position $\mathbf{y}_c$: we replace $j_s^{\text{in}}(\mathbf{x}, t)$ by $p(t)\delta(\mathbf{x} - \mathbf{y}_c)$. The function $p(t)$ corresponds to the waveform transmitted from the antenna [21].

If we write the waveform p in terms of its Fourier transform P,

$$p(t) = \frac{1}{2\pi} \int \mathrm{e}^{-\mathrm{i}\omega t} P(\omega)\, \mathrm{d}\omega, \tag{21}$$

and use the Green's function g from (20), we find that E^{in} satisfies

$$E^{\mathrm{in}}(\mathbf{x}, t) = g * j_s(\mathbf{x}, t) = g * [p(t)\delta(\mathbf{x} - \mathbf{y}_c)] \tag{22}$$

$$= \int \frac{\mathrm{e}^{-\mathrm{i}\omega(t - n(\omega)|\mathbf{x} - \mathbf{y}_c|/c_0)}}{16\pi^3 |\mathbf{x} - \mathbf{y}_c|} P(\omega)\, \mathrm{d}\omega. \tag{23}$$

Here the $*$ denotes convolution in both space and time.

Next, we assume that the center of the antenna $\mathbf{y}_c$ is moving along the curve γ. Thus, we replace $\mathbf{y}_c$ by a parametric curve

$$\gamma := \{\gamma(s) \in \mathbb{R}^3 : s \in (s_{\min}, s_{\max}) \subset \mathbb{R}\}. \tag{24}$$

Here we use the fact that the time scale on which the antenna moves is very different from the time scale on which the electromagnetic waves propagate. This allows us to introduce a new time parameter s, called the *slow time*, which describes the position of the antenna along its flight path. In doing so, we are assuming that the movement of the antenna can be neglected during the time it takes for a pulse to propagate through the scene and back to the antenna. This is called the *start-stop approximation*. Thus, expression (22) depends also on the slow time s:

$$E^{\mathrm{in}}(\mathbf{x}, t, s) = \int \frac{\mathrm{e}^{-\mathrm{i}\omega(t - n(\omega)|\mathbf{x} - \gamma(s)|/c_0)}}{16\pi^3 |\mathbf{x} - \gamma(s)|} P(\omega)\, \mathrm{d}\omega. \tag{25}$$

2.4.2. The scattered field. The scattered field E^{sc} satisfies

$$\begin{aligned} \nabla^2 E^{\mathrm{sc}} - \partial_t^2 \big(c_0^{-2} \varepsilon_r \underset{t}{*} E^{\mathrm{sc}}\big) &= -j^{\mathrm{sc}}(t, \boldsymbol{x}) = -\int v(t - t', \boldsymbol{x}) E^{\mathrm{tot}}(t', \boldsymbol{x})\, \mathrm{d}t' \\ &= -\int T(x_1, x_2)\delta(\mathbf{x} - \boldsymbol{\Psi}(x_1, x_2))\partial_t^2 \delta(t - t') E^{\mathrm{tot}}(t', \boldsymbol{x})\, \mathrm{d}t' \\ &= -T(x_1', x_2')\delta(\mathbf{x}' - \boldsymbol{\psi}(x_1', x_2'))\partial_t^2 E^{\mathrm{tot}}(t, \boldsymbol{x}). \end{aligned} \tag{26}$$

The Green's function (20) then allows us to write the solution E^{sc} of (26) as

$$E^{\mathrm{sc}}(\mathbf{x}, t, s) = \int g(\mathbf{x} - \mathbf{x}', t - \tau) T(x_1', x_2') \delta(\mathbf{x}' - \boldsymbol{\Psi}(x_1', x_2')) \partial_\tau^2 E^{\mathrm{tot}}(\mathbf{x}', \tau, s)\, \mathrm{d}\tau\, \mathrm{d}\mathbf{x}'. \tag{27}$$

This equation is the *Lippmann–Schwinger equation*. It defines a nonlinear mapping from a target T to the associated scattered field $E^{\mathrm{sc}}(\mathbf{x}, t, s)$. The nonlinearity arises because $E^{\mathrm{tot}} = E^{\mathrm{in}} + E^{\mathrm{sc}}$ on the right-hand side of (27) also depends on T. We will now proceed to linearize (27).

2.4.3. Linearized data model. If we replace the full field E^{tot} on the right-hand side of (27) by the incident field E^{in}, we get the *Born approximation* or the *single-scattering approximation* to the scattered field

$$E_B^{\mathrm{sc}}(\mathbf{x}, t, s) := \int g(\mathbf{x} - \mathbf{x}', t - \tau) T(x_1', x_2') \delta(\mathbf{x}' - \boldsymbol{\Psi}(x_1', x_2')) \partial_\tau^2 E^{\mathrm{in}}(\mathbf{x}', \tau, s)\, \mathrm{d}\tau\, \mathrm{d}\mathbf{x}'. \tag{28}$$

We have used a subscript B to indicate that we are using the Born approximation. This approximation removes the nonlinearity of (27) by replacing the product of T and E^{tot} by the

product of T and the known incident field. The Born approximation is valid when the average intensity of the scattered field E^{sc} is small compared to the average intensity of the incident field E^{in} in a given volume ($|E^{\mathrm{sc}}| \ll |E^{\mathrm{in}}|$) [22].

We now substitute Green's function (20) and the incident field (25) into (28), to obtain the scattered wavefield

$$E_B^{\mathrm{sc}}(\mathbf{x}, t, s) = \int \frac{\mathrm{e}^{-\mathrm{i}\omega\left(t - n(\omega)(|\mathbf{x}-\boldsymbol{\Psi}(x_1', x_2')| + |\boldsymbol{\Psi}(x_1', x_2') - \boldsymbol{\gamma}(s)|)/c_0\right)}}{(16\pi^3)^2 |\mathbf{x} - \boldsymbol{\Psi}(x_1', x_2')||\boldsymbol{\Psi}(x_1', x_2') - \boldsymbol{\gamma}(s)|} \times \omega^2 P(\omega) T(x_1', x_2') \Lambda(x_1', x_2') \,\mathrm{d}\omega \,\mathrm{d}x_1' \,\mathrm{d}x_2', \tag{29}$$

where

$$\Lambda(x_1, x_2) = \sqrt{1 + \left(\frac{\partial \psi}{\partial x_1}\right)^2 + \left(\frac{\partial \psi}{\partial x_2}\right)^2} \tag{30}$$

accounts for the surface area on non-planar topography. We introduce a *modified target*

$$\tilde{T}(\boldsymbol{y}) := T(\boldsymbol{y}) \Lambda(\boldsymbol{y}) \tag{31}$$

in (29):

$$E_B^{\mathrm{sc}}(\mathbf{x}, t, s) = \int \frac{\mathrm{e}^{-\mathrm{i}\omega\left(t - n(\omega)(|\mathbf{x}-\boldsymbol{\Psi}(x_1', x_2')| + |\boldsymbol{\Psi}(x_1', x_2') - \boldsymbol{\gamma}(s)|)/c_0\right)}}{(16\pi^3)^2 |\mathbf{x} - \boldsymbol{\Psi}(x_1', x_2')||\boldsymbol{\Psi}(x_1', x_2') - \boldsymbol{\gamma}(s)|} \times \omega^2 P(\omega) \tilde{T}(x_1', x_2') \,\mathrm{d}\omega \,\mathrm{d}x_1' \,\mathrm{d}x_2'. \tag{32}$$

To keep notation simpler, we will omit the tilde, and just write T. We should keep in mind, though, that formulas in the remainder of this paper are for the modified target. For flat topography, there is no distinction.

We will measure the scattering data using the same antenna as was used to transmit the waveform $p(t)$. By setting $\mathbf{x} = \boldsymbol{\gamma}(s)$ in (32), we obtain

$$E_B^{\mathrm{sc}}(\boldsymbol{\gamma}(s), t, s) = \int \frac{\mathrm{e}^{-\mathrm{i}\omega(t - 2n(\omega)|\mathbf{r}_{s,y}|/c_0)}}{(16\pi^3)^2 |\mathbf{r}_{s,y}|^2} \omega^2 P(\omega) T(\boldsymbol{y}) \,\mathrm{d}\omega \,\mathrm{d}\boldsymbol{y}. \tag{33}$$

In (33) we have introduced a bold italic font for 2D vector positions; i.e. $\boldsymbol{y} := \{(y_1, y_2) \in \mathbb{R}^2\}$ and $\mathrm{d}\boldsymbol{y}$ is the 2D surface measure, and we have used the vector $\mathbf{r}_{s,y}$:

$$\mathbf{r}_{s,y} := \boldsymbol{\Psi}(\boldsymbol{y}) - \boldsymbol{\gamma}(s). \tag{34}$$

Equation (33) describes the scattering data in terms of a linear mapping, which we denote by F, from the target to the scattered electric field. Thus, $E_B^{\mathrm{sc}}(\gamma(s), t, s) = \mathrm{F}(T)(t, s)$. Finally, we will include additive noise $\eta(t, s)$ in our data model:

$$d(t, s) := \mathrm{F}(T)(t, s) + \eta(t, s). \tag{35}$$

3. Image formation

We will now form the image $I(\boldsymbol{z})$, i.e. an approximation to $T(\boldsymbol{z})$. In the previous works on dispersionless media [13–15, 21], the image formation strategy used the fact that the mapping F from the reflectivity function T to the scattered electric field took the form of a Fourier integral operator (FIO) (see [23]). The tools of microlocal analysis were used to construct an approximate inversion operator and to analyze the regularity of the reconstructed image. In the case of dispersion, however, the forward operator is not a FIO because of the nonlinear dependence of the phase on the frequency ω. Nevertheless, we follow a similar strategy for

image formation, namely looking for an inverse as a modified version of the filtered adjoint of the forward operator.

To form an image $I(\boldsymbol{z})$ (i.e. an approximation to $T(\boldsymbol{z})$), we apply to the noisy data (35) an operator M_Q of the form

$$I(\boldsymbol{z}) = \mathrm{M}_Q(d) := \int \mathrm{e}^{\mathrm{i}\omega'\left(t - 2n_R(\omega')|\mathbf{r}_{s,z}|/c_0\right)} Q(\omega', \boldsymbol{z}, s)\, \mathrm{d}\omega'\, \mathrm{d}(t, s)\, \mathrm{d}t\, \mathrm{d}s. \tag{36}$$

An important feature here is that the explicit phase of (36) involves only the real part $n_R(\omega)$. Because the real part corresponds to the correct propagation speed, this results in a back-projection method which places the scatterers at the correct spatial range. The role of Q will be to enhance edges, while controlling noise contributions to the image. We will determine Q in such a way as to minimize the variance in the 'edge-information' (i.e. the leading-order terms) in the reconstructed image.

3.1. Image fidelity

To determine the relationship between the formed image I and the true target T, we substitute (35) and (33) into (36):

$$\begin{aligned} I(\boldsymbol{z}) = \int & \mathrm{e}^{-\mathrm{i}2\left(\omega' n_R(\omega')|\mathbf{r}_{s,z}| - \omega n_R(\omega)|\mathbf{r}_{s,y}|\right)/c_0} Q(\omega', \boldsymbol{z}, s)\, \mathrm{e}^{-\mathrm{i}(\omega-\omega')t}\, \mathrm{d}t \\ & \times \frac{\mathrm{e}^{-2\omega n_I(\omega)|\mathbf{r}_{s,y}|/c_0}}{(4\pi|\mathbf{r}_{s,y}|)^2} \omega^2 P(\omega) T(\boldsymbol{y})\, \mathrm{d}\omega'\, \mathrm{d}\omega\, \mathrm{d}\boldsymbol{y}\, \mathrm{d}s \\ & + \int \mathrm{e}^{-\mathrm{i}\left(2\omega' n_R(\omega')|\mathbf{r}_{s,z}|/c_0 - \omega' t\right)} Q(\omega', \boldsymbol{z}, s)\, \mathrm{d}\omega' \eta(t, s)\, \mathrm{d}t\, \mathrm{d}s. \end{aligned} \tag{37}$$

In the first integral, we can perform the integration with respect to t, and subsequently with respect to ω to obtain

$$\begin{aligned} I(\boldsymbol{z}) = & \int \mathrm{e}^{-\mathrm{i}2\omega n_R(\omega)\left(|\mathbf{r}_{s,z}| - |\mathbf{r}_{s,y}|\right)/c_0} Q(\omega, s, \boldsymbol{z}) \frac{\mathrm{e}^{-2\omega n_I(\omega)|\mathbf{r}_{s,y}|/c_0}}{(16\pi^3|\mathbf{r}_{s,y}|)^2} \omega^2 P(\omega)\, \mathrm{d}\omega T(\boldsymbol{y})\, \mathrm{d}\boldsymbol{y}\, \mathrm{d}s \\ & + \int \mathrm{e}^{-\mathrm{i}\left(2\omega n_R(\omega)|\mathbf{r}_{s,z}|/c_0 - \omega t\right)} Q(\omega, s, \boldsymbol{z}) \eta(t, s)\, \mathrm{d}t\, \mathrm{d}\omega\, \mathrm{d}s. \end{aligned} \tag{38}$$

We have here dropped the prime on ω' in the second integral. The image is therefore divided into two parts, namely a target term I_T and a noise term I_η:

$$I(\boldsymbol{z}) = I_T(\boldsymbol{z}) + I_\eta(\boldsymbol{z}). \tag{39}$$

Here

$$I_T(\boldsymbol{z}) := \int \mathrm{e}^{-\mathrm{i}2\omega n_R(\omega)\left(|\mathbf{r}_{s,z}| - |\mathbf{r}_{s,y}|\right)/c_0} Q(\omega, s, \boldsymbol{z}) \frac{\mathrm{e}^{-2\omega n_I(\omega)|\mathbf{r}_{s,y}|/c_0}}{(16\pi^3|\mathbf{r}_{s,y}|)^2} \omega^2 P(\omega)\, \mathrm{d}\omega T(\boldsymbol{y})\, \mathrm{d}\boldsymbol{y}\, \mathrm{d}s, \tag{40}$$

and

$$I_\eta(\boldsymbol{z}) := \int \mathrm{e}^{-\mathrm{i}\left(2\omega n_R(\omega)|\mathbf{r}_{s,z}|/c_0 - \omega t\right)} Q(\omega, s, \boldsymbol{z}) \eta(t, s)\, \mathrm{d}t\, \mathrm{d}\omega\, \mathrm{d}s. \tag{41}$$

Our goal is to design Q in such a way as to suppress noise while simultaneously retaining as much of the target information as possible.

In order to simplify notation, we make the following definitions:

$$\vartheta_R(\omega) := 2\omega n_R(\omega)/c_0, \tag{42}$$

$$A(\omega, s, \boldsymbol{y}) := \frac{\omega^2\, \mathrm{e}^{-2\omega n_I(\omega)|\mathbf{r}_{s,y}|/c_0}}{(16\pi^3|\mathbf{r}_{s,y}|)^2}, \tag{43}$$

$$A_P(\omega, s, \boldsymbol{y}) := A(\omega, s, \boldsymbol{y})P(\omega). \tag{44}$$

With this notation, we rewrite (38) as

$$I(\boldsymbol{z}) = \int \mathrm{e}^{-\mathrm{i}\vartheta_R(\omega)[|\mathbf{r}_{s,z}|-|\mathbf{r}_{s,y}|]} Q(\omega, s, \boldsymbol{z}) A_P(\omega, s, \boldsymbol{y}) T(\boldsymbol{y})\, \mathrm{d}\omega\, \mathrm{d}\boldsymbol{y}\, \mathrm{d}s \tag{45a}$$

$$+ \int \mathrm{e}^{-\mathrm{i}[\vartheta_R(\omega)|\mathbf{r}_{s,z}|-\omega t]} Q(\omega, s, \boldsymbol{z}) \eta(t, s)\, \mathrm{d}t\, \mathrm{d}\omega\, \mathrm{d}s. \tag{45b}$$

We assume that the product QA_P of (45*a*) is sufficiently well behaved for the integral to converge and for the method of stationary phase to be applicable. More specifically, we assume that the product QA_P satisfies the symbol estimates [23]. Consequently, we can apply the method of stationary phase (see appendix B) to the ω and s integrals of (45*a*) to find that the leading-order contributions to (45*a*) stem from the critical points, which satisfy

$$|\mathbf{r}_{s,z}| = |\mathbf{r}_{s,y}| \tag{46}$$

$$\widehat{\mathbf{r}_{s,z}} \cdot \gamma(s) = \widehat{\mathbf{r}_{s,y}} \cdot \gamma(s). \tag{47}$$

Here $\widehat{\mathbf{r}_{s,z}} = \frac{\mathbf{r}_{s,z}}{|\mathbf{r}_{s,z}|}$. Thus, we see that the leading-order contributions to the image arise only from those points $\boldsymbol{z}$ whose range (46) and Doppler shift (47) are the same as those for $\boldsymbol{y}$.

We assume that (46) and (47) have solutions only when $\boldsymbol{z} = \boldsymbol{y}$. Whether this is true depends on the topography, flight path and antenna beam pattern. This assumption holds, for example, for a side-looking radar system flying in a straight line over flat topography, and was discussed extensively in [13].

In a neighborhood of $\boldsymbol{z} = \boldsymbol{y}$, we simplify the phase of the exponent in (45*a*) using the integral form of the remainder for Taylor's theorem. As in [13], we use the identity

$$h(\boldsymbol{z}) - h(\boldsymbol{y}) = (\boldsymbol{z} - \boldsymbol{y}) \cdot \int_0^1 \nabla h(\boldsymbol{y} - \lambda(\boldsymbol{z} - \boldsymbol{y}))\, \mathrm{d}\lambda, \tag{48}$$

with $h(\boldsymbol{z}) = \vartheta_R(\omega)|\mathbf{r}_{s,z}|$ to write the exponent of (45*a*) as

$$\vartheta_R(\omega)[|\mathbf{r}_{s,z}| - |\mathbf{r}_{s,y}|] = (\boldsymbol{z} - \boldsymbol{y}) \cdot \Xi(\omega, s, \boldsymbol{z}, \boldsymbol{y}), \tag{49}$$

where

$$\Xi(\omega, s, \boldsymbol{z}, \boldsymbol{y}) = \vartheta_R(\omega) \int_0^1 \nabla_{\boldsymbol{x}} |\mathbf{r}_{s,\boldsymbol{x}}| \Big|_{\boldsymbol{x}=\boldsymbol{y}+\lambda(\boldsymbol{z}-\boldsymbol{y})} \mathrm{d}\lambda. \tag{50}$$

For each $\boldsymbol{z}$ and $\boldsymbol{y}$, we make the Stolt change of variables

$$(\omega, s) \mapsto \boldsymbol{\xi} := -\Xi(\omega, s, \boldsymbol{z}, \boldsymbol{y}), \tag{51}$$

and write the corresponding Jacobian as

$$J(s, \omega, \boldsymbol{y}, \boldsymbol{z}) := \left| \frac{\partial(s, \omega)}{\partial \boldsymbol{\xi}} \right|, \tag{52}$$

such that

$$\mathrm{d}\omega\, \mathrm{d}s = \left| \frac{\partial(\omega, s)}{\partial \boldsymbol{\xi}} \right| \mathrm{d}\boldsymbol{\xi} = J(\boldsymbol{\xi}, \boldsymbol{z}, \boldsymbol{y})\, \mathrm{d}\boldsymbol{\xi}. \tag{53}$$

The absolute value of this determinant is often referred to as the *Beylkin determinant*. In appendix C, we derive its reciprocal:

$$\left| \frac{\partial \boldsymbol{\xi}}{\partial(\omega, s)} \right| = \left| \frac{4\omega}{v_p(\omega) v_g(\omega)} \det \begin{bmatrix} \widehat{\mathbf{r}^0_{s,z}} \cdot \partial_{z_1} \boldsymbol{\Psi} & P_\perp \dot{\gamma}(s) \cdot \partial_{z_1} \boldsymbol{\Psi} \\ \widehat{\mathbf{r}^0_{s,z}} \cdot \partial_{z_2} \boldsymbol{\Psi} & P_\perp \dot{\gamma}(s) \cdot \partial_{z_2} \boldsymbol{\Psi} \end{bmatrix} \right|, \tag{54}$$

where the phase velocity, v_p, was defined in (7), and the *group velocity*, v_g, is defined as

$$v_g(\omega) := \frac{c_0}{n_R(\omega) + \omega\partial_\omega n_R(\omega)}. \tag{55}$$

The Stolt change of variables (51) can be performed (locally) as long as the right-hand side of (54) is nonzero [13]. Thus, for the analysis below, we need an additional criterion which is strictly related to the dispersive nature of the medium, namely that the first factor of (54) should be nonzero:

$$\frac{4\omega}{v_p(\omega)v_g(\omega)} \neq 0. \tag{56}$$

For example, this requirement is certainly satisfied for media exhibiting *normal dispersion* [24], where $\partial_\omega n_R(\omega) > 0$.

By performing the change of variables (51) in the first integral, we transform (3.1) into

$$I(\boldsymbol{z}) = \int \mathrm{e}^{\mathrm{i}(\boldsymbol{z}-\boldsymbol{y})\cdot\boldsymbol{\xi}} Q(\boldsymbol{\xi}, \boldsymbol{z}) A_P(\boldsymbol{\xi}, \boldsymbol{y}) T(\boldsymbol{y}) J(\boldsymbol{\xi}, \boldsymbol{z}, \boldsymbol{y})\, \mathrm{d}\boldsymbol{\xi}\, \mathrm{d}\boldsymbol{y} \tag{57}$$

$$+ \int \mathrm{e}^{-\mathrm{i}[\vartheta_R(\omega)|\mathbf{r}_{s,z}|-\omega t]} Q(\omega, s, \boldsymbol{z}) \eta(t, s)\, \mathrm{d}t\, \mathrm{d}\omega\, \mathrm{d}s. \tag{58}$$

3.2. Determination of filter Q

When $\boldsymbol{z} = \boldsymbol{y}$, $\boldsymbol{\xi}$ becomes $-\Xi(\omega, s, \boldsymbol{z}, \boldsymbol{z})$, where

$$\Xi(\omega, s, \boldsymbol{z}, \boldsymbol{z}) := \vartheta_R(\omega)\widehat{\mathbf{r}_{s,z}} \cdot D\boldsymbol{\Psi}(\boldsymbol{z}), \tag{59}$$

and $D\boldsymbol{\Psi}$ is the Jacobian matrix. We denote by Ω_z the set of values that $\boldsymbol{\xi}$ can take on:

$$\Omega_z = \{\boldsymbol{\xi} = -\vartheta_R(\omega)\widehat{\mathbf{r}_{s,z}} \cdot D\boldsymbol{\Psi}(\boldsymbol{z}) \in \mathbb{R}^2 : \omega \in (\omega_{\min}, \omega_{\max}) \text{ and } s \in (s_{\min}, s_{\max})\}. \tag{60}$$

(Note that for flat topography, multiplying the vector $\widehat{\mathbf{r}_{s,z}}$ on the right-hand side by the matrix $D\boldsymbol{\Psi}(\boldsymbol{z})$ simply projects the unit vector $\widehat{\mathbf{r}_{s,z}}$ onto the flat plane.) On Ω_z, we write the Jacobian (53) as

$$J(\omega, s, \boldsymbol{z}) := J(\omega, s, \boldsymbol{z}, \boldsymbol{z}). \tag{61}$$

The set Ω_z is called the *data-collection manifold*, and is determined via the Stolt change of variables (51) by the flight path and the frequency band. The set Ω_z identifies the Fourier components of T that are present in the data. The size of the set Ω_z determines the resolution of the imaging system (see [15] for further details).

In an L^2 sense, the best reconstruction of T from Fourier components in Ω_z is obtained by restricting the Fourier transform of T to Ω_z before performing the inverse Fourier transform:

$$I_{\Omega_z}(\boldsymbol{z}) = \int_{\Omega_z} \mathrm{e}^{\mathrm{i}(\boldsymbol{z}-\boldsymbol{y})\cdot\boldsymbol{\xi}} T(\boldsymbol{y})\, \mathrm{d}\boldsymbol{\xi}. \tag{62}$$

We will use this as the *ideal image* against which our reconstruction will be compared.

3.2.1. Image variance, bias and expected mean-square error. We will now proceed to determine the filter Q for which the image I obtained using (36) is the best reconstruction. For this purpose we will quantify the quality of each reconstruction using the L^2-norm of the deviation between our reconstruction and the reference reconstruction given by (62). If we define the point-wise error $\mathcal{E}(\boldsymbol{z})$,

$$\mathcal{E}(\boldsymbol{z}) := I(\boldsymbol{z}) - I_{\Omega_z}(\boldsymbol{z}), \tag{63}$$

then the L^2 error for this reconstruction is

$$\Delta(Q, P, T) := \int |\mathcal{E}(\boldsymbol{z})|^2 \, \mathrm{d}\boldsymbol{z}. \tag{64}$$

Due to the presence of additive random noise, the reconstructed image is, strictly speaking, a stochastic quantity, which implies that (64) is also stochastic. Furthermore, rather than designing a Q which performs well for any particular reflectivity function T, we want a Q that performs well for a family of reflectivity functions. We therefore average the error over this family of candidate reflectivities. More specifically, we will consider each target as a realization of a random field. The stochastic noise model and the random field model for the target induce a probability density function for $\Delta(Q, P, T)$. Rather than using (64), we therefore proceed to use the mean-square error (MSE) as a measure of reconstruction error:

$$\Delta(Q, P) := \langle \Delta(Q, P, T) \rangle = \left\langle \int |\mathcal{E}(\boldsymbol{z})|^2 \, \mathrm{d}\boldsymbol{z} \right\rangle. \tag{65}$$

Here we have used $\langle \cdot \rangle$ to indicate expectation. We can of course interchange expectation and integration in (65) to obtain the mean-square error expressed as an integral over the point-wise second-order moment of the reconstruction error

$$\Delta(Q, P) = \int \langle |\mathcal{E}(\boldsymbol{z})|^2 \rangle \, \mathrm{d}\boldsymbol{z}. \tag{66}$$

The MSE comprises two components (for details see [15] and [25]):

$$\Delta(Q, P) = \mathcal{V}(Q, P) + \mathcal{B}(Q, P), \tag{67}$$

where $\mathcal{V}(Q, P)$ is the total variance of $\mathcal{E}$:

$$\mathcal{V}(Q, P) := \int \langle |\mathcal{E}(\boldsymbol{z}) - \langle \mathcal{E}(\boldsymbol{z}) \rangle|^2 \rangle \, \mathrm{d}\boldsymbol{z}, \tag{68}$$

and $\mathcal{B}(Q, P)$ is the square of the L^2-norm of the bias:

$$\mathcal{B}(Q, P) := \int |\langle I(\boldsymbol{z}) \rangle - \langle I_{\Omega_z}(\boldsymbol{z}) \rangle|^2 \, \mathrm{d}\boldsymbol{z}. \tag{69}$$

It is well known that in general we cannot expect to obtain an image with both correct mean and minimal variance. Because it is very desirable that the image does not change appreciably for different realizations of noise, we minimize the variance of the image, but do not constrain the mean.

In the rest of the paper, for simplicity, we address the case in which the target T has a zero mean. Since the scattering model and the reconstruction algorithm both are linear, this implies that the expected value for the reconstruction is also zero; in this case the bias term is zero. In this case, minimizing the MSE is equivalent to minimizing the variance. We therefore proceed to minimize the MSE of (66), keeping in mind that for our case this is equivalent to minimizing the variance. Furthermore, the same results are obtained if there is a known non-zero mean; minimizing the variance amounts to subtracting off the mean and then minimizing the mean-square error.

Assumption 3.1 (Stochastic scattering)**.** *We assume that the target T is a zero-mean second-order random field with known covariance function R_T:*

$$\langle T(\boldsymbol{y}) \rangle = 0 \tag{70}$$

$$R_T(\boldsymbol{y}, \boldsymbol{y}') := \langle T(\boldsymbol{y}) \overline{T(\boldsymbol{y}')} \rangle. \tag{71}$$

Here $\overline{T(\boldsymbol{y}')}$ is the complex conjugate of $T(\boldsymbol{y}')$. Furthermore, we assume that the noise $\eta(t, s)$ is a zero-mean second-order stochastic process [26, 27] which (a) is stationary in the fast-time

variable t, (b) is statistically uncorrelated in the slow-time variable s and (c) has a spectral density function S_η which we define through the relation

$$\int \mathrm{e}^{\mathrm{i}\omega t_1}\,\mathrm{e}^{-\mathrm{i}\omega' t_2}\langle\overline{\eta(t_1,s)}\eta(t_2,s')\rangle\,\mathrm{d}t_1\,\mathrm{d}t_2 = S_\eta(\omega,s)\delta(\omega-\omega')\delta(s-s'). \tag{72}$$

Here again bar denotes complex conjugation. Finally we assume that the T and η are statistically independent such that

$$\langle T(\boldsymbol{y})\overline{\eta(t,s)}\rangle = \langle T(\boldsymbol{y})\rangle\overline{\langle\eta(t,s)\rangle} = 0. \tag{73}$$

Under these assumptions, the best image in the minimum MSE sense is obtained by minimizing the integral

$$\Delta(P,Q) = \int \langle|I(\boldsymbol{z}) - I_{\Omega_z}(\boldsymbol{z})|^2\rangle\,\mathrm{d}\boldsymbol{z} = \Delta_T(P,Q) + \Delta_\eta(P,Q), \tag{74}$$

where, omitting functional dependence on P and Q,

$$\Delta_T = \int\left\langle\left|\int_{\Omega_z}\mathrm{e}^{\mathrm{i}(\boldsymbol{z}-\boldsymbol{y})\cdot\boldsymbol{\xi}}Q(\boldsymbol{\xi},\boldsymbol{z})A_P(\boldsymbol{\xi},\boldsymbol{y})T(\boldsymbol{y})J(\boldsymbol{\xi},\boldsymbol{z})\,\mathrm{d}\boldsymbol{\xi}\,\mathrm{d}\boldsymbol{y} - I_{\Omega_z}(\boldsymbol{z})\right|^2\right\rangle\mathrm{d}\boldsymbol{z} \tag{75}$$

and

$$\Delta_\eta = \left\langle\int \mathrm{e}^{-\mathrm{i}[\vartheta_R(\omega)|\mathbf{r}_{s,z}|-\omega t]}Q(\omega,s,\boldsymbol{z})\eta(t,s)\,\mathrm{d}t\,\mathrm{d}\omega\,\mathrm{d}s \times\int \mathrm{e}^{\mathrm{i}[\vartheta_R(\omega')|\mathbf{r}_{s',z}|-\omega' t']}\overline{Q(\omega',s',\boldsymbol{z})\eta(t',s')}\,\mathrm{d}t'\,\mathrm{d}\omega'\,\mathrm{d}s'\right\rangle\mathrm{d}\boldsymbol{z}. \tag{76}$$

Note that the cross terms vanish in (74) because the target and the noise are statistically independent and have zero mean. Rearranging (76), we obtain

$$\Delta_\eta = \int \mathrm{e}^{-\mathrm{i}[\vartheta_R(\omega)|\mathbf{r}_{s,z}|-\vartheta_R(\omega')|\mathbf{r}_{s',z}|]}Q(\omega,s,\boldsymbol{z})\overline{Q(\omega',s',\boldsymbol{z})} \tag{77}$$

$$\times\int \mathrm{e}^{-\mathrm{i}\omega t}\,\mathrm{e}^{i'\omega t'}\langle\eta(t,s)\overline{\eta(t',s')}\rangle\,\mathrm{d}t'\,\mathrm{d}t\,\mathrm{d}\omega'\,\mathrm{d}s'\,\mathrm{d}\omega\,\mathrm{d}s\,\mathrm{d}\boldsymbol{z}. \tag{78}$$

Using the noise properties (72) in (77), we arrive at

$$\Delta_\eta = \int |Q(\omega,s,\boldsymbol{z})|^2 S_\eta(\omega,s)\,\mathrm{d}\omega\,\mathrm{d}s\,\mathrm{d}\boldsymbol{z}. \tag{79}$$

We expand and rewrite expression (75) to get

$$\Delta_T = \iint_{\Omega_z\times\Omega_z}\mathrm{e}^{\mathrm{i}[(\boldsymbol{z}-\boldsymbol{y})\cdot\boldsymbol{\xi}-(\boldsymbol{z}-\boldsymbol{y}')\cdot\boldsymbol{\xi}']}u(\boldsymbol{\xi},\boldsymbol{\xi}',\boldsymbol{y},\boldsymbol{y}',\boldsymbol{z})R_T(\boldsymbol{y},\boldsymbol{y}')\,\mathrm{d}\boldsymbol{\xi}\,\mathrm{d}\boldsymbol{\xi}'\,\mathrm{d}\boldsymbol{y}\,\mathrm{d}\boldsymbol{y}'\,\mathrm{d}\boldsymbol{z}, \tag{80}$$

where

$$u = [Q(\boldsymbol{\xi},\boldsymbol{z})A_P(\boldsymbol{\xi},\boldsymbol{y})J(\boldsymbol{\xi},\boldsymbol{z}) - 1][\overline{Q(\boldsymbol{\xi}',\boldsymbol{z})A_P(\boldsymbol{\xi}',\boldsymbol{y}')J(\boldsymbol{\xi}',\boldsymbol{z}) - 1}]. \tag{81}$$

Here bar denotes complex conjugate.

To simplify (80), we apply the stationary phase approximation [23] to the phase $(\boldsymbol{z}-\boldsymbol{y})\cdot\boldsymbol{\xi} - (\boldsymbol{z}-\boldsymbol{y}')\cdot\boldsymbol{\xi}'$, where the critical set and the Hessian are (see appendix B)

$$\text{Critical set}\begin{cases}\dfrac{\partial\phi}{\partial\boldsymbol{z}} = \boldsymbol{\xi}-\boldsymbol{\xi}' = 0\\[2ex] \dfrac{\partial\phi}{\partial\boldsymbol{\xi}'} = -(\boldsymbol{z}-\boldsymbol{y}') = 0\end{cases}\qquad\text{Hessian}\left\{\frac{\partial^2\phi}{\partial\boldsymbol{z}\partial\boldsymbol{\xi}'} = \begin{pmatrix}0 & -I\\ -I & 0\end{pmatrix}.\right. \tag{82}$$

Consequently, the main contribution to the integral (80) comes from the set $\boldsymbol{\xi}' = \boldsymbol{\xi}$ and $\boldsymbol{z} = \boldsymbol{y}'$:

$$\Delta_T \sim \iint_{\Omega_z} \mathrm{e}^{\mathrm{i}(z-y)\cdot\xi}\,[Q(\boldsymbol{\xi},\boldsymbol{z})A_P(\boldsymbol{\xi},\boldsymbol{y})J(\boldsymbol{\xi},\boldsymbol{z})-1] \times \overline{[Q(\boldsymbol{\xi},\boldsymbol{z})A_P(\boldsymbol{\xi},\boldsymbol{z})J(\boldsymbol{\xi},\boldsymbol{z})-1]}R_T(\boldsymbol{y},\boldsymbol{z})\,\mathrm{d}\boldsymbol{\xi}\,\mathrm{d}\boldsymbol{y}\,\mathrm{d}\boldsymbol{z}. \tag{83}$$

Let us now define S_T through the following Fourier transform relation with R_T:

$$R_T(\boldsymbol{y},\boldsymbol{z}) = \iint \mathrm{e}^{-\mathrm{i}y\cdot\zeta}\,\mathrm{e}^{\mathrm{i}z\cdot\zeta'}\,S_T(\zeta,\zeta')\,\mathrm{d}\zeta\,\mathrm{d}\zeta'. \tag{84}$$

We will refer to S_T as the *target spectral-density function*. Inserting (84) into (83) we arrive at

$$\Delta_T \sim \iint_{\Omega_z} \mathrm{e}^{\mathrm{i}[(z-y)\cdot\xi+y\cdot\zeta-z\cdot\zeta']}\,[Q(\boldsymbol{\xi},\boldsymbol{z})A_P(\boldsymbol{\xi},\boldsymbol{y})J(\boldsymbol{\xi},\boldsymbol{z})-1] \times \overline{[Q(\boldsymbol{\xi},\boldsymbol{z})A_P(\boldsymbol{\xi},\boldsymbol{z})J(\boldsymbol{\xi},\boldsymbol{z})-1]}S_T(\zeta,\zeta')\,\mathrm{d}\zeta\,\mathrm{d}\zeta'\,\mathrm{d}\boldsymbol{\xi}\,\mathrm{d}\boldsymbol{y}\,\mathrm{d}\boldsymbol{z}. \tag{85}$$

To (85) we again apply the method of stationary phase. In this case the phase is $\boldsymbol{z}\cdot(\boldsymbol{\xi}-\zeta') - \boldsymbol{y}\cdot(\boldsymbol{\xi}-\zeta)$, and the leading-order contribution comes from the points $\boldsymbol{\xi} = \zeta'$ and $\boldsymbol{z} = \boldsymbol{y}$. The leading-order term is

$$\Delta_T \sim \iint_{\Omega_z} \mathrm{e}^{\mathrm{i}z\cdot(\zeta-\xi)}\,|Q(\boldsymbol{\xi},\boldsymbol{z})A_P(\boldsymbol{\xi},\boldsymbol{z})-1|^2\,S_T(\zeta,\xi)|J(\boldsymbol{\xi},\boldsymbol{z})|^2\,\mathrm{d}\zeta\,\mathrm{d}\boldsymbol{\xi}\,\mathrm{d}\boldsymbol{z}. \tag{86}$$

We now make the assumption that the target T is a wide-sense stationary random field. In this case, the correlation function R_T is a function only of the difference between its two variables:

$$S_T(\zeta,\xi) = S_T(\zeta)\delta(\zeta-\xi). \tag{87}$$

Under this assumption, from (86) we obtain

$$\Delta_T \sim \iint_{\Omega_z} |Q(\boldsymbol{\xi},\boldsymbol{z})A_P(\boldsymbol{\xi},\boldsymbol{z})J(\boldsymbol{\xi},\boldsymbol{z})-1|^2\,S_T(\boldsymbol{\xi})\,\mathrm{d}\boldsymbol{\xi}\,\mathrm{d}\boldsymbol{z}. \tag{88}$$

We now revert to the original coordinates $\boldsymbol{\xi} \to (\omega, s)$; by undoing the Stolt change of variables in (88), we get

$$\Delta_T \sim \int |Q(\omega,s,\boldsymbol{z})A_P(\omega,s,\boldsymbol{z})J(\omega,s,\boldsymbol{z})-1|^2\,S_T(\boldsymbol{\xi}(\omega,s,\boldsymbol{z}))\frac{\mathrm{d}\omega\,\mathrm{d}s}{J(\omega,s,\boldsymbol{z})}\,\mathrm{d}\boldsymbol{z}. \tag{89}$$

Combining (89) and (79), we get the following integral expression for the variance in the reconstruction:

$$\Delta(P,Q) \sim \int |Q(\omega,s,\boldsymbol{z})A_P(\omega,s,\boldsymbol{z})J(\omega,s,\boldsymbol{z})-1|^2\,\frac{S_T(\boldsymbol{\xi}(\omega,s,\boldsymbol{z}))}{J(\omega,s,\boldsymbol{z})}\,\mathrm{d}\omega\,\mathrm{d}s\,\mathrm{d}\boldsymbol{z} \tag{90a}$$

$$+ \int |Q(\omega,s,\boldsymbol{z})|^2 S_\eta(\omega,s)\,\mathrm{d}\omega\,\mathrm{d}s\,\mathrm{d}\boldsymbol{z}. \tag{90b}$$

We want to find the optimal filter $Q = Q^{\mathrm{opt}}$ for which (90) is minimized. To do this, we set to zero the variational derivative of $\Delta(P,Q)$ with respect to Q:

$$\begin{aligned} 0 = \left.\frac{\mathrm{d}}{\mathrm{d}\rho}\right|_{\rho=0} \Delta(P,Q^{\mathrm{opt}}+\rho q) &\sim \left.\frac{\mathrm{d}}{\mathrm{d}\rho}\right|_{\rho=0} \int |(Q^{\mathrm{opt}}+\rho q)A_P J - 1|^2 \frac{S_T}{J}\,\mathrm{d}\omega\,\mathrm{d}s\,\mathrm{d}\boldsymbol{z} \\ &+ \left.\frac{\mathrm{d}}{\mathrm{d}\rho}\right|_{\rho=0} \int |Q^{\mathrm{opt}}+\rho q|^2 S_\eta\,\mathrm{d}\omega\,\mathrm{d}s\,\mathrm{d}\boldsymbol{z} \\ &= \int 2\,\mathrm{Re}\{\overline{q\,A_P J}[(Q^{\mathrm{opt}}+\rho q)A_P J - 1]\}\Big|_{\rho=0} \frac{S_T}{J}\,\mathrm{d}\omega\,\mathrm{d}s\,\mathrm{d}\boldsymbol{z} \end{aligned}$$

$$+\int 2\,\mathrm{Re}\{\overline{q}(Q^{\mathrm{opt}}+\rho q)\}\Big|_{\rho=0} S_\eta \,\mathrm{d}\omega\,\mathrm{d}s\,\mathrm{d}\boldsymbol{z}$$

$$=\int 2\left(\mathrm{Re}\{\overline{qA_PJ}[A_PJQ^{\mathrm{opt}}-1]\}\frac{S_T}{J}+\mathrm{Re}\{\overline{q}Q^{\mathrm{opt}}\}S_\eta\right)\mathrm{d}\omega\,\mathrm{d}s\,\mathrm{d}\boldsymbol{z}. \tag{91}$$

As this should hold for all q, we obtain

$$(|A_P|^2Q^{\mathrm{opt}}J-\overline{A_P})S_T+Q^{\mathrm{opt}}S_\eta=0. \tag{92}$$

Solving for Q^{opt}, we find that

$$Q^{\mathrm{opt}}(\omega,s,\boldsymbol{z})=\frac{\overline{A_P(\omega,s,\boldsymbol{z})}}{|A_P(\omega,s,\boldsymbol{z})|^2J(\omega,s,\boldsymbol{z})+S_\eta(\omega,s)/S_T(\boldsymbol{\xi}(\omega,s,\boldsymbol{z}))}. \tag{93}$$

Finally, we use (44) to substitute back $A_P(\omega,s,\boldsymbol{z})=A(\omega,s,\boldsymbol{z})P(\omega,s)$. We summarize this result in the following theorem.

Theorem 3.2 (Optimal reconstruction filter)**.** *Let the background medium satisfy assumptions 2.1. Let the stochastic target model satisfy assumptions 3.1. In (36), the filter Q that is optimal, in the sense of minimizing the variance (90) in the leading-order contributions of the image, is given by*

$$Q^{\mathrm{opt}}(\omega,s,\boldsymbol{z})=\frac{\overline{A(\omega,s,\boldsymbol{y})P(\omega)}}{|A(\omega,s,\boldsymbol{y})P(\omega)|^2J(\omega,s,\boldsymbol{z})+\sigma_{\eta T}(\omega,s)}, \tag{94}$$

where the (frequency-domain) noise-to-target ratio $\sigma_{\eta T}$ is defined as

$$\sigma_{\eta T}(\omega,s,\boldsymbol{z}):=S_\eta(\omega,s)/S_T(\omega,s,\boldsymbol{z}), \tag{95}$$

and we have used (51) to define $S_T(\omega,s,\boldsymbol{z})$:

$$S_T(\omega,s,\boldsymbol{z}):=S_T(\xi(\omega),s,\boldsymbol{z}), \tag{96}$$

and A is given by (43).

For the non-dispersive case, we see that our reconstruction is identical to the variance-minimizing filter which was derived in [15], though the results therein were stated as filtering integrations over the image frequency variable ξ. Here, we have chosen to express the filter as a function of the data collection variables (ω,s) directly, to reduce any confusion as to how the filter is applied.

Four special cases of (94) are worth noting.

(i) *No noise:* $\sigma_{\eta T}=0$, then the filter (94) reduces to the inverse filter $(APJ)^{-1}$. In the non-dispersive case this becomes the filter which was derived in [13].

(ii) *No signal:* if the target does not scatter waves in some frequency interval, i.e. if $S_T(\xi(\omega,s,\boldsymbol{z}))=0$ for some ω interval, then formally $\sigma_{\eta T}$ is infinite and $Q^{\mathrm{opt}}=0$; the filter does not pass frequencies in this interval and therefore there is no contribution to the image from these frequencies, see equations (57) and (58).

(iii) *Non-zero signal and noise spectrum:* in the case of non-zero noise-to-target spectrum ratio, the filter is appropriately weighted [28, 29]. The quantity $\sigma_{\eta T}$ is a frequency-dependent *regularization term*.

(iv) *White noise:* if the noise can be assumed to be spectrally white and independent of the slow-time parameter s, equation (94) reduces to a simple parametric filter

$$Q^{\mathrm{opt}}(\omega,s,\boldsymbol{z})=\frac{S_T\overline{AP}}{|AP|^2JS_T+\sigma^2}, \tag{97}$$

with a constant σ^2 equal to the noise variance.

3.3. Noise-to-target and signal-to-noise ratios

The optimal reconstruction filter depends on a somewhat unconventional quantity, namely the noise-to-target ratio $\sigma_{\eta T}$. It is more common to refer to the signal-to-noise ratio (SNR); we show below how the noise-to-target ratio is related to the SNR.

From (33), we see that in the Fourier domain, the signal without noise is

$$D_T(\omega, s) = \int \frac{\mathrm{e}^{2\mathrm{i}\omega n(\omega)|\mathbf{r}_{s,y}|/c_0}}{(4\pi|\mathbf{r}_{s,y}|)^2}\omega^2 P(\omega)T(\boldsymbol{y})\,\mathrm{d}\boldsymbol{y}. \tag{98}$$

Therefore, the signal variance is

$$\langle|D_T(\omega, s)|^2\rangle = \omega^4|P(\omega)|^2 \int \frac{\mathrm{e}^{\mathrm{i}\omega 2n(\omega)|\mathbf{r}_{s,y}|/c_0}\,\mathrm{e}^{-\mathrm{i}\omega 2n(\omega)|\mathbf{r}_{s,y'}|/c_0}}{(4\pi^2|\mathbf{r}_{s,y}|)^2(4\pi^2|\mathbf{r}_{s,y'}|)^2}\langle T(\boldsymbol{y})\overline{T(\boldsymbol{y}')}\rangle\,\mathrm{d}\boldsymbol{y}'\,\mathrm{d}\boldsymbol{y}. \tag{99}$$

If we assume that the flight path is far from the targets, i.e. $|\boldsymbol{r}_{s,y}|$ and $|\boldsymbol{r}_{s,y'}|$ are large, then we can perform a far-field approximation in (98) to obtain

$$\begin{aligned}\langle|D_T(\omega, s)|^2\rangle \approx{}& \left(\frac{\omega^2|P(\omega)|}{4\pi^2|\boldsymbol{r}_{s,y}|^2}\right)^2 \mathrm{e}^{-4|\boldsymbol{r}_{s,y}|\omega n_I(\omega)/c_0} \\ &\times \int \mathrm{e}^{-2\omega n_R(\omega)/c_0 \frac{\boldsymbol{r}_{s,y}}{|\boldsymbol{r}_{s,y}|}\cdot(\boldsymbol{y}'-\boldsymbol{y})} R_T(\boldsymbol{y}-\boldsymbol{y}')\,\mathrm{d}\boldsymbol{y}\,\mathrm{d}\boldsymbol{y}'.\end{aligned} \tag{100}$$

We recognize the integration as a Fourier transform which takes the target correlation function R_T into the target spectral density S_T:

$$\langle|D_T(\omega, s)|^2\rangle \approx \left(\frac{\omega^2|P(\omega)|}{4\pi^2|\boldsymbol{r}_{s,y}|^2}\right)^2 \mathrm{e}^{-4|\boldsymbol{r}_{s,y}|\omega n_I(\omega)/c_0} S_T\left(2\omega n_R(\omega)/c_0 \frac{\boldsymbol{r}_{s,y}}{|\boldsymbol{r}_{s,y}|}\right). \tag{101}$$

If $\boldsymbol{y}$ is at the origin, we can use (51) and (C.13) to see that this is indeed

$$\underbrace{\frac{\langle|D_T(\omega, s)|^2\rangle}{S_\eta(\omega, s)}}_{\text{SNR}} \approx \left(\frac{\omega^2|P(\omega)|}{4\pi^2|\boldsymbol{r}_{s,y}|^2}\right)^2 \mathrm{e}^{-4|\boldsymbol{r}_{s,y}|\omega n_I(\omega)/c_0} \underbrace{\frac{S_T\left(-\Xi(s, \omega, 0, 0)\right)}{S_\eta(\omega, s)}}_{1/\sigma_{\eta T}}. \tag{102}$$

We can therefore view the SNR as approximately $1/\sigma_{\eta T}$, multiplied by the square of the amplitude of the signal which is received after being scattered from a target with unit reflectivity.

An important difference between the SNR and the noise-to-target ratio is that the SNR depends on the distance from the target region to the flight path, whereas the noise-to-target ratio does not.

4. Numerical simulations

Now we present numerical simulations which illustrate the algorithm introduced in the previous section. The scene consists of a homogeneous background with embedded point reflectors. These reflectors are *weak scatterers* in the sense that their permittivity is close to that of the background medium. The trajectory for the radar antenna is a circular path with a radius of 100 m, at a height 10 m above the flat ground. Figure 2 shows an illustration of this scenario.

The transmitted waveform which we used was a sinusoid with carrier frequency 0.1 GHz. This value was chosen so as to coincide with the frequency band where the index of refraction displays most change (see figure 4). The sinusoid was truncated to a pulse length of 85 ns. In order to keep the effective support of the pulse spectrum within the band of frequencies

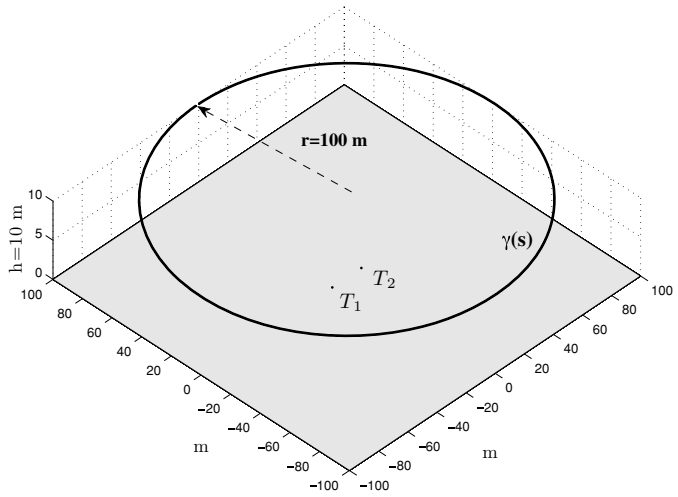

Figure 2. Radar scene and antenna trajectory. The radar antenna follows a circular trajectory with a radius of 100 m, at a height of 10 m above a flat ground. The background is homogeneous, and the target consists of two point reflectors.

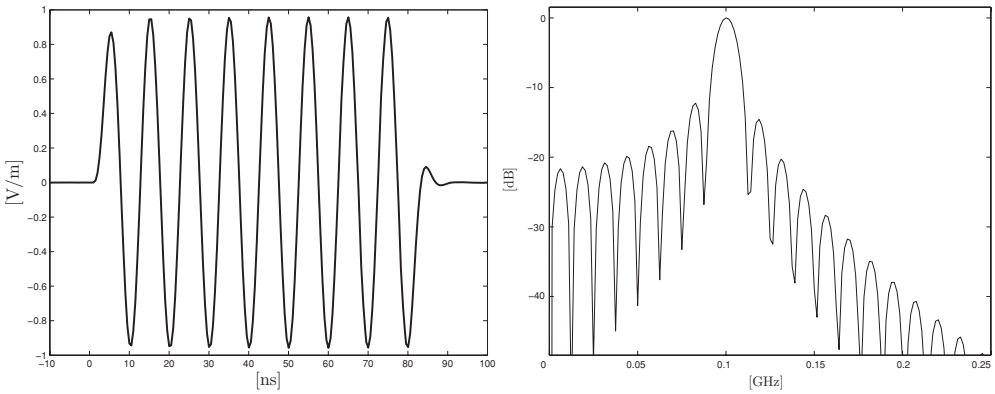

Figure 3. Transmit waveform which was radiated into the scene. Left: time-domain waveform. Right: spectrum of transmit waveform.

permitted by our temporal sampling rate, we applied a low-pass filter to the waveform. The result can be seen in figure 3. We observe the effect of the low-pass filter as a smooth modulation of the sinusoid.

Noise was added to the scattering simulations to emulate electronic receiver noise. For this we used a noise model with constant power spectrum, namely white Gaussian noise. The noise level was kept constant along the full trajectory, and chosen to yield a given average time-domain SNR. For this we used the following definition of average time-domain SNR:

$$\text{average time-domain SNR} := \sup_t \frac{1}{(2\pi)^2} \int \mathrm{e}^{-\mathrm{i}\omega t} \frac{\langle |S(\omega, s)|^2 \rangle}{S_\eta(\omega, s)} \, \mathrm{d}\omega \, \mathrm{d}s, \quad (103)$$

where $S(\omega, s)$ is the temporal Fourier transform of the noiseless scattering modeled by (33), and S_η is the noise spectrum.

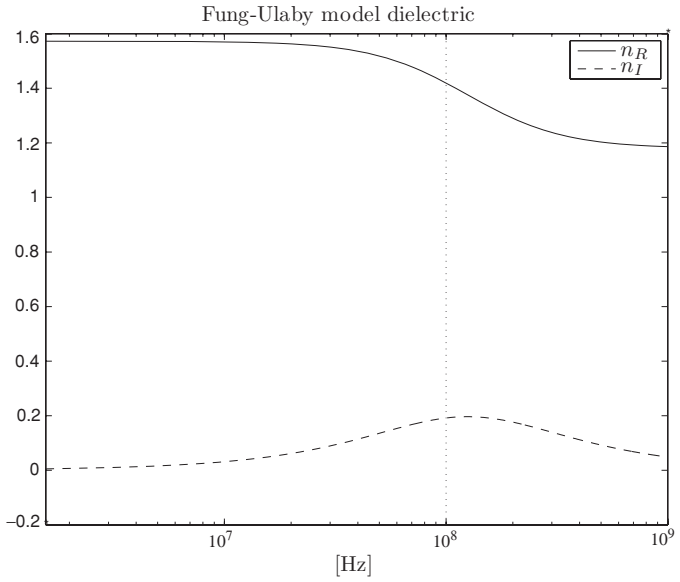

Figure 4. Profile of the real and imaginary parts of the complex-valued refractive index with a time-relaxation parameter modeled according to the Fung–Ulaby model with relaxation time $\tau = 8$ ns. The leaf and water fraction parameters are $v_l = 0.04$ and $v_w = 0.2$, respectively. The vertical dotted line shows the center frequency of the transmitted waveform.

When reconstructing the image, we need, in addition to the noise spectrum, an expression for the target spectrum. Information about approximate target location, scattering strength or spatial correlation between different targets could be encoded into this spectrum. For our purposes, we chose to consider independent point reflectors, and a white target spectrum; the function $S_T(\xi)$ is a constant.

In all simulations, the background consisted of leafy vegetation, which we modeled with the Fung–Ulaby model (see appendix A and [30]). This model involves three parameters: the concentration of leaves v_l in a given volume of air, the percentage of water v_w present in each leaf and the relaxation time τ of water.

4.1. Sparse vegetation

To model sparse foliage, we took $v_w = 0.20$ (20% of the weight of each leaf is water), $v_l = 0.04$ (4% of the given volume of air is filled by leaves) and $\tau = 8$ ns. These parameters were chosen so that condition (56) is satisfied in the entire frequency band. In figure 4 we show the profile of the real and imaginary parts of the index of refraction (square root of the Fung–Ulaby permittivity).

Figure 5 shows scattering simulations with average time-domain SNR of 40 dB and with 0 dB. The leading and trailing edge transients which are clearly visible in the 40 dB SNR case are called Brillouin precursors [1, 8]. These transient wavefields have been studied extensively and, because with increasing propagation distance, they decay algebraically rather than exponentially, such Brillouin precursors have been considered potentially useful for foliage- and ground-penetrating radar as well for underwater communications (for details see [31–33]).

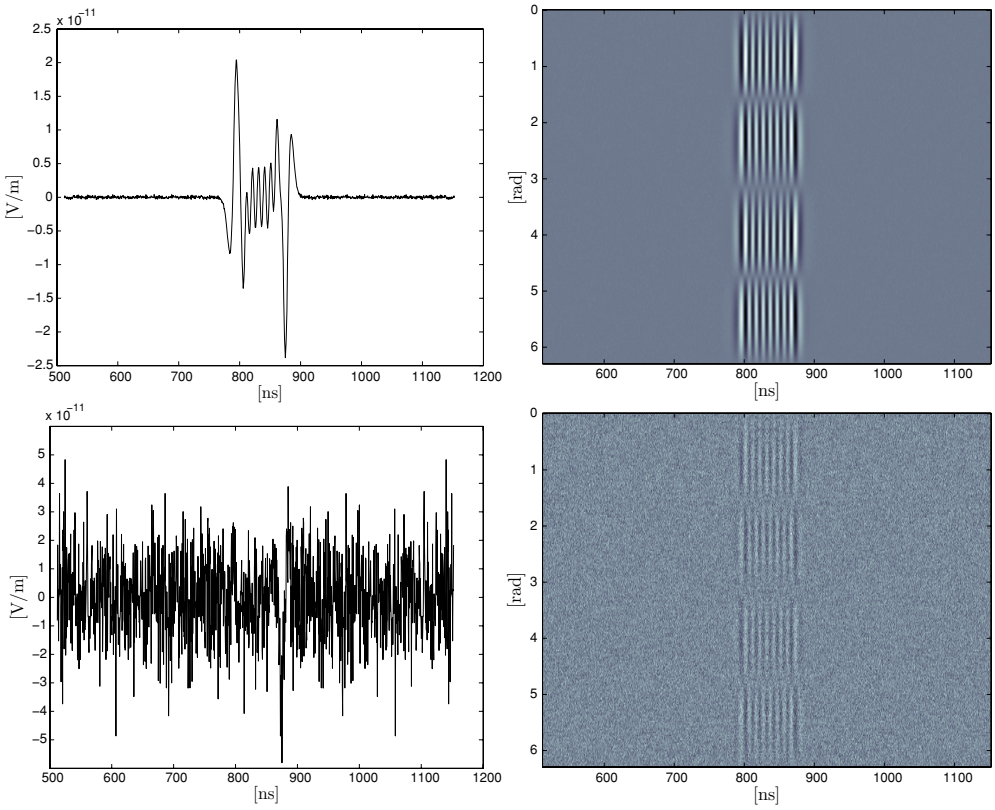

Figure 5. Simulated scattering measurements from two point reflectors. White noise has been added to yield a SNR of 40 dB in the top row, and 0 dB in the bottom row.

Figure 7 shows reconstructions for varying levels of SNR. For comparison, the same reconstructions were also performed from scattering measured in a non-dispersive medium. We see clearly how the dispersion degrades the spatial resolution; this can be understood as follows. It is common knowledge that the spatial resolution is proportional to the bandwidth. It is, however, not necessarily the bandwidth of the transmit pulse that is important; note that here the transmit pulse was the same for all cases. The important quantity is what we refer to as the effective bandwidth, i.e., the bandwidth of the resulting signal after it has been filtered. This incorporates both the effect of dispersion and the effect of the noise. For our simulations, this bandwidth is simply the intersection of the bandwidth of the filter,

$$W(\boldsymbol{z}, \omega) := \frac{|AP|^2 S_T}{|AP|^2 J S_T + \sigma^2}, \tag{104}$$

with the set of frequencies $|\boldsymbol{\xi}|$ obtained from (60). In figure 6 we see the effective bandwidth of (104) for $\boldsymbol{z} = \mathbf{0}$ (the origin), plotted as the width of the frequency band where $W(\mathbf{0}, \omega)$ exceeds -6 dB of its maximum. It is clear from this plot that increasing the noise level will decrease the effective bandwidth. Furthermore, dispersion clearly affects the bandwidth; dispersion affects high frequencies more than low frequencies. In the high-frequency range the noise is therefore more dominant in the dispersive case than in the non-dispersive case.

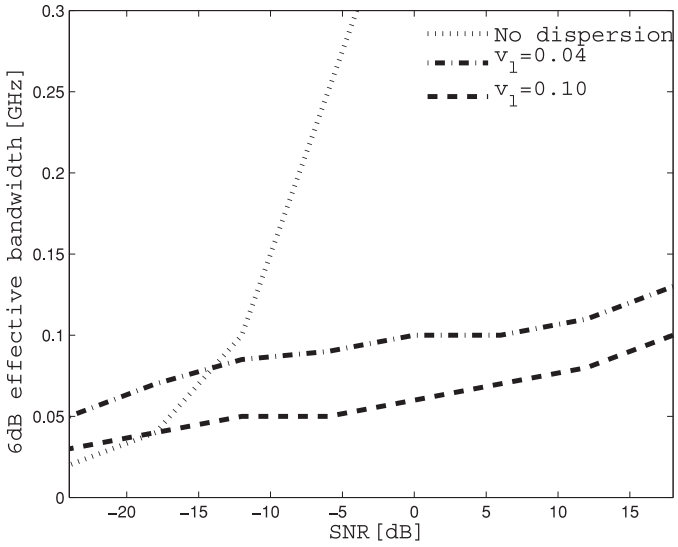

Figure 6. Effective bandwidth used in the reconstruction.

Curiously, for the extremely low SNR, the bandwidth seems to be better for the dispersive case than for the non-dispersive case. This can be explained by the fact that dispersion renders the main lobe of the measured signal broader and flatter than the transmitted signal. This results in a broader, -6 dB frequency width when only the main lobe is included in the calculations.

Moreover, as the SNR decreases from virtually noise-free data to a SNR of -30 dB, the images become blurry, and lose contrast. Note how the ability to recover the peak strength decreases with the increasing amount of regularization which is applied as the SNR decreases. Here the colorbars in the right column of figure 7 have been normalized with respect to those on the left.

In general, the noise-to-target ratio (NTR) is a function of spatial location, as well as frequency and location on the flight path. For the simulations performed here, where both the noise and target spectral densities are constant, the NTR reduces to a single number. For the permittivity corresponding to 4% foliage volume fraction and a range of about 100 m, a 40 dB SNR corresponds to a 55 dB NTR, and -20 dB SNR corresponds to 115 dB NTR.

4.2. Dense vegetation

To model dense vegetation, we take the leaf volume fraction to be $v_l = 0.1$ and $v_w = 0.20$ (20% of the weight of each leaf is water) and $\tau = 8$ ns. The corresponding index of refraction is shown in figure 8.

In figure 9 we see the scattering measurements from two point scatterers. The leading and trailing edge transients which are clearly visible in figure 9 are the Brillouin precursors.

In figure 10, we show the reconstructed images for the 40, 0, -20 and -30 dB SNR. When the SNR = -20 dB, the two point scatterers are completely lost by blurring.

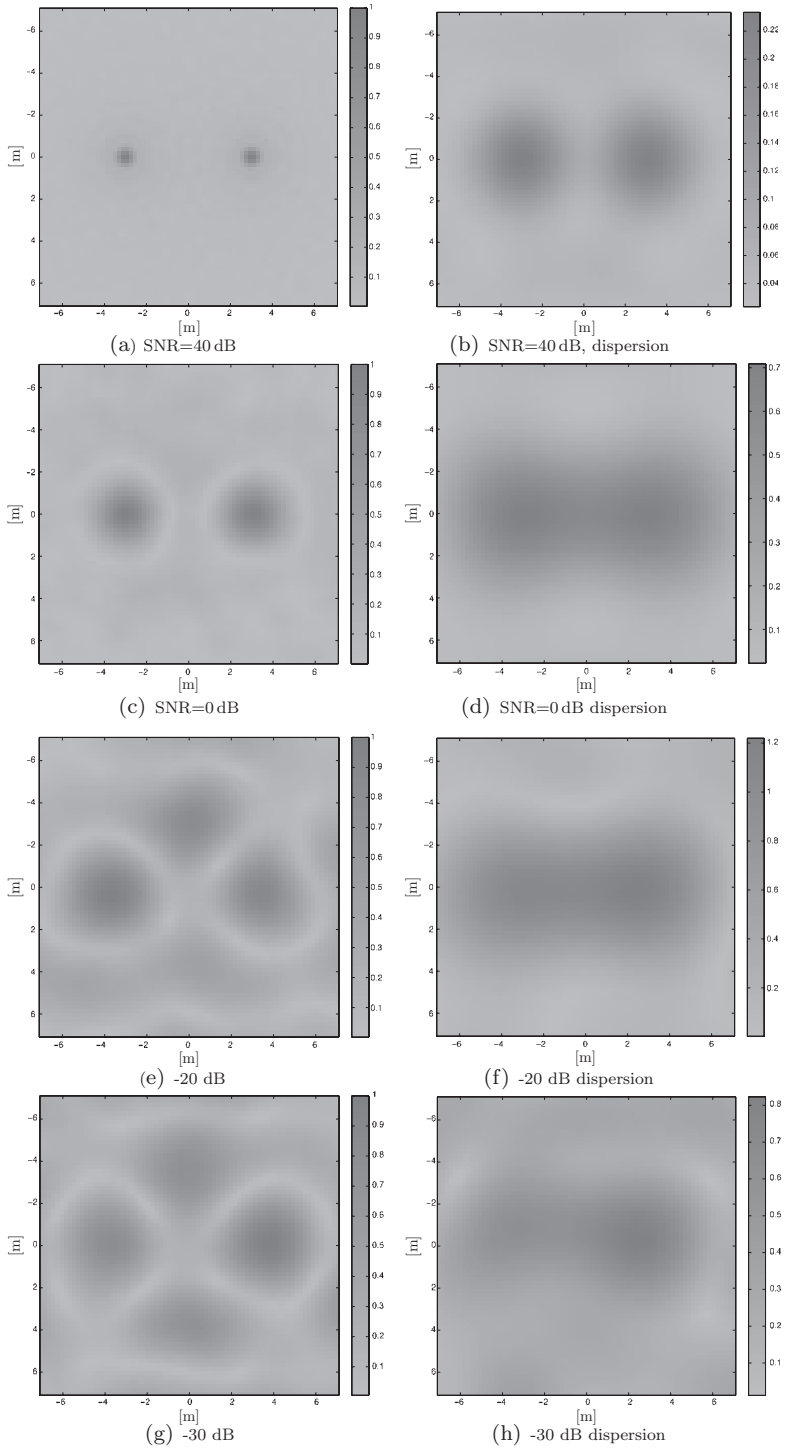

(a) SNR=40 dB (b) SNR=40 dB, dispersion

(c) SNR=0 dB (d) SNR=0 dB dispersion

(e) -20 dB (f) -20 dB dispersion

(g) -30 dB (h) -30 dB dispersion

Figure 7. Reconstructed images of two point reflectors located at coordinates $(-3, 0)$ and $(3, 0)$ based on noisy measurements. The amplitude scale of the images has been normalized with respect to the non-dispersive case. Left column: non-dispersive background. Right column: dispersive background when $v_l = 0.04$.

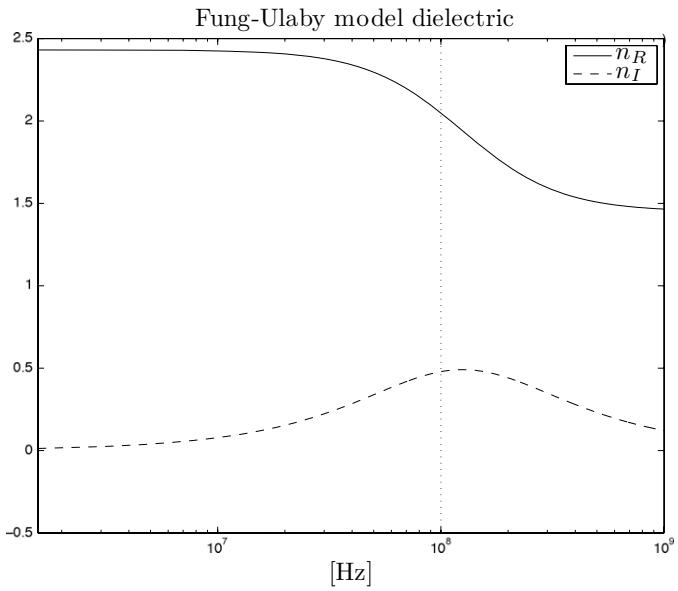

Figure 8. Profile of the real and imaginary parts of the complex-valued refractive index in the case of dense vegetation. The parameters in the Fung–Ulaby model are $\tau = 8$ ns, $v_l = 0.1$ and $v_w = 0.2$. The vertical dotted line indicates the frequency of the transmitted waveform.

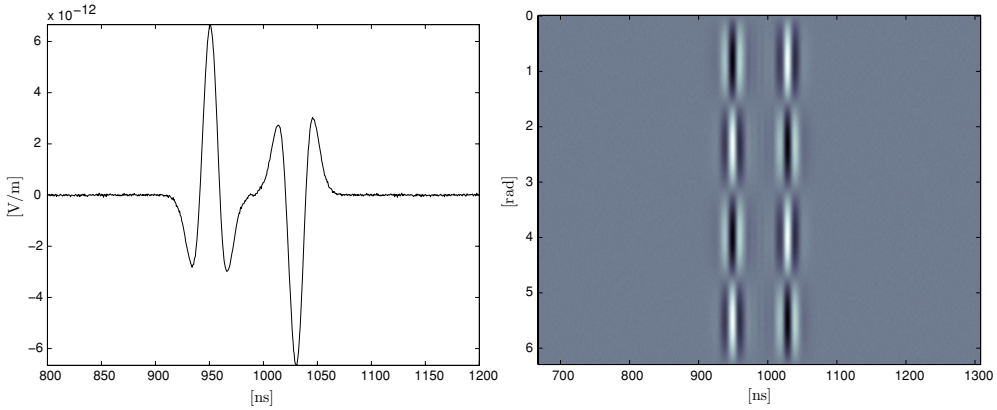

Figure 9. Simulated scattering measurements from two point reflectors in a dense vegetation background.

5. Concluding remarks

In this paper, we have developed a formula for forming SAR images through a temporally dispersive medium. For a given waveform, we derived a filtered-back-projection reconstruction method, the filter of which was optimally designed to minimize the reconstruction error in the mean-square sense. Thus, this paper has extended the analysis in [13] and [15] to the situation where the background is dispersive. In the non-dispersive case, the filter we derive here reduces to the one found in [15].

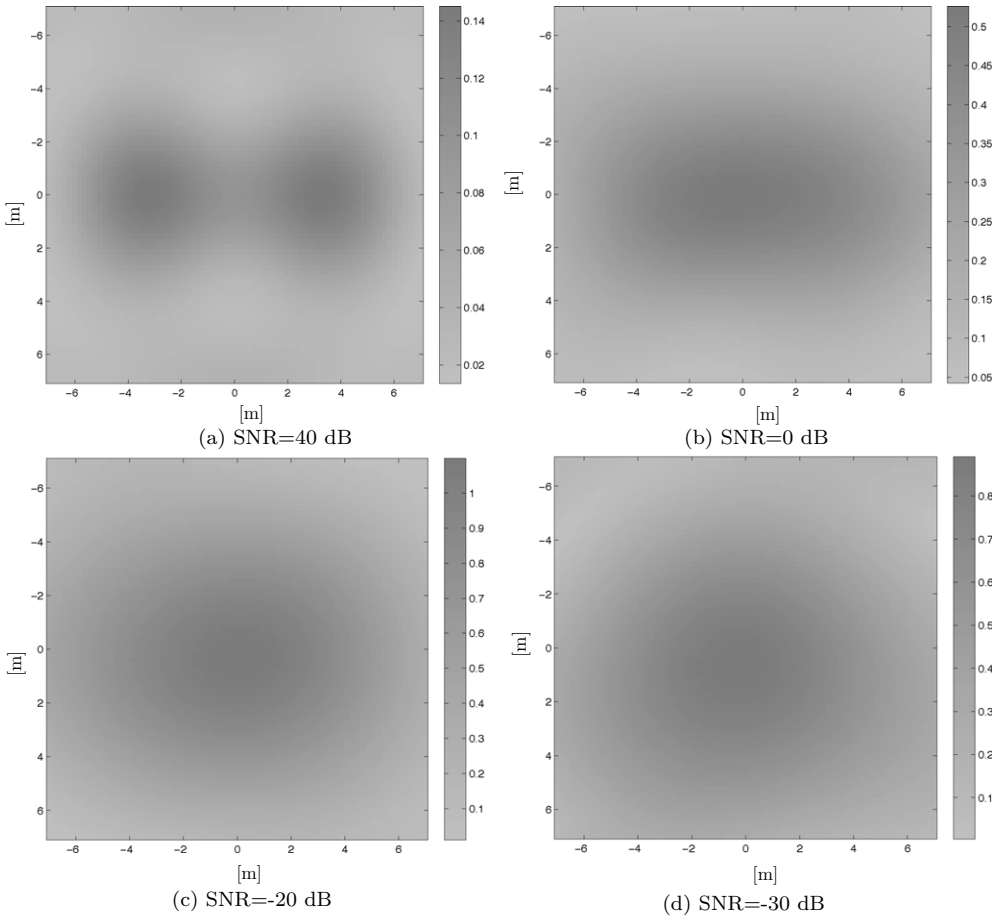

Figure 10. Reconstructed images of two point reflectors located at coordinates $(-3, 0)$ and $(3, 0)$ in a dispersive medium based on noisy measurements when $v_l = 0.1$. The amplitude scale of the images has been normalized with respect to its corresponding (not shown) non-dispersive case images.

We note that although the analysis here uses the Stolt change of variables, and therefore requires the Beylkin determinant to be non-singular, the resulting reconstruction filter is well defined also in the case of a singular Beylkin determinant; we see from (94) that a singular Beylkin determinant merely results in certain frequencies not being passed through the filter.

We showed reconstructions from this method for the case of a transmitted waveform consisting of a square-wave-modulated sine wave. In the future we will address the issue of optimal waveform design for improving imaging through a dispersive medium.

Acknowledgments

We are grateful to Richard Albanese for suggesting the problem and for contributing many constructive comments. We also thank Brett Borden for suggesting this approach to deriving the scattering model, and Kurt Oughstun for making a number of helpful comments. We are

grateful to Air Force Office of Scientific Research[4] (AFOSR) for supporting this work under the agreements FA9550-06-1-0017 and FA9550-09-1-0013. JHM acknowledges support from The National Council for Science and Technology (CONACyT) of Mexico.

Appendix A. The Fung–Ulaby model

In our numerical examples, we used the model for complex-valued permittivity developed by Fung and Ulaby [30] for vegetation. In this model, the permittivity of the vegetation (taken to be a combination of water and some solid material) was estimated by a mixing formula for two-phase mixtures [34, 35]. The effective relative permittivity is given by

$$\epsilon_{r,\mathrm{eff}}(\omega) = v_l \epsilon_l + (1 - v_l), \tag{A.1}$$

where $\epsilon_l = \epsilon_R(\omega) + \mathrm{i}\,\epsilon_I(\omega)$, and

$$\epsilon_R(\omega) = 5.5 + \frac{e_m - 5.5}{1 + \tau^2\omega^2}, \qquad \epsilon_I(\omega) = \frac{(e_m - 5.5)\tau\omega}{1 + \tau^2\omega^2},$$

where $e_m = 5 + 51.56 v_m$, where v_l is the fractional volume occupied by leaves, v_w is the water volume fraction within a 'typical leaf' and τ is an empirical relaxation time of water molecules. The relaxation time τ is governed by the interaction of the water molecules with its environment and by the temperature T. The relaxation time for pure water at 20 °C is $\tau \approx 10.1 \times 10^{-12}$ s.

In order to perform the Stolt change of variables, we need to make sure that the frequency band of the transmit waveform does not contain a frequency for which the condition (56) is violated. For the Fung–Ulaby model we have

$$2n_R \frac{\partial n_R}{\partial \omega} = \mathrm{Re}\left[\frac{\partial \epsilon_r}{\partial \omega}\right] = -\frac{2(e_m - 5.5)\tau^2\omega}{(1 + \tau^2\omega^2)^2}. \tag{A.2}$$

Inserting $e_m = 5 + 51.86 v_m$, and substituting the result into (56), we have

$$\frac{\partial n_R}{\partial \omega} = -\frac{2(51.86 v_m - 0.5)\tau^2\omega}{(1 + \tau^2\omega^2)^2}. \tag{A.3}$$

Thus, we see that (56) is equivalent to

$$1 \neq \frac{2(51.86 v_m - 0.5)\tau^2\omega^2}{(1 + \tau^2\omega^2)^2}. \tag{A.4}$$

Inserting the relaxation time $\tau = 10.1 \times 10^{-12}$ s into (A.4), we find that condition (56) holds for all frequencies as long as the volume fraction is smaller than about 0.048. For higher volume fractions, there will be two frequencies for which condition (A.4) does not hold.

Appendix B. The method of stationary phase

In this appendix we show how to use the method of stationary phase to approximate the integral (80). This integral is of the type

$$I(\lambda) = \int \mathrm{e}^{\mathrm{i}\lambda\phi(\boldsymbol{x})} u(\boldsymbol{x})\,\mathrm{d}\boldsymbol{x}. \tag{B.1}$$

[4] Consequently, the US Government is authorized to reproduce and distribute reprints for governmental purposes notwithstanding any copyright notation thereon. The views and conclusions contained herein are those of the authors and should not be interpreted as necessarily representing the official policies or endorsements, either expressed or implied, of the Air Force Research Laboratory or the US Government.

The stationary phase method deals with integrals of the form (B.1) in which the integration is over a compact set K in $\mathbb{R}^N$. The point $\boldsymbol{x}_l \in K$ is a *critical point* if $\nabla\phi(\boldsymbol{x}_l) = 0$. A critical point $\boldsymbol{x}_l$ is *non-degenerate* if $\det(D^2\phi(\boldsymbol{x}_l)) \neq 0$, where $D^2\phi(\boldsymbol{x}) = \left(\frac{\partial^2\phi(\boldsymbol{x})}{\partial x_j \partial x_k}\right)_{1\leqslant j,k\leqslant N}$ is the Hessian of ϕ at $\boldsymbol{x}$.

The stationary phase theorem states that if $u \in C_0^\infty(K)$, and ϕ has only non-degenerate critical points $\{\boldsymbol{x}_1, \boldsymbol{x}_2, \ldots\}$, then as $\lambda \to \infty$ the leading-order approximation to (B.1) is obtained from the estimate (see proposition 2.3 in [23])

$$\left| I(\lambda) - \left(\frac{2\pi}{\lambda}\right)^{N/2} \sum_l R_l u(\boldsymbol{x}_l)\, \mathrm{e}^{\mathrm{i}\lambda\phi(\boldsymbol{x}_l)} \right| \leqslant \frac{C}{\lambda^{1+(N/2)}} \sum_{|\kappa|\leqslant N+3} \left(\sup_K |\partial^\kappa u(\boldsymbol{x})|\right), \tag{B.2}$$

where $\lambda \geqslant 1$, $\kappa = (\kappa_1, \kappa_2, \ldots, \kappa_N)$, $\partial^\kappa = \partial_{x_1}^{\kappa_1}\partial_{x_2}^{\kappa_2}\cdots\partial_{x_N}^{\kappa_N}$, where

$$R_l = \frac{\mathrm{e}^{\mathrm{i}\pi\,\mathrm{sgn}(D^2\phi(\boldsymbol{x}_l))/4}}{|\det D^2\phi(\boldsymbol{x}_l)|^{1/2}}, \tag{B.3}$$

and where $\mathrm{sgn}(\cdot)$ denotes the signature of the Hessian, i.e., the number of positive eigenvalues minus the number of negative ones.

If ϕ and u depend on parameters, the same result holds provided that u satisfies a symbol estimate of the form given in [23].

Leading-order behavior of (45a). Into (40) or (45*a*), we introduce a large parameter λ as follows. In (45*a*), first we make the change of variables

$$\omega \mapsto \nu := \vartheta_R(\omega). \tag{B.4}$$

Assume that ν is a smooth function, which satisfies $\partial_\omega \nu \neq 0$ for all $\omega \in \mathbb{R}$. (This condition is satisfied by the Fung–Ulaby model, where we also have $\nu = \mathcal{O}(\omega)$ for large ω.) This ensures that the change of variables is globally well defined, so we re-write (45*a*) as

$$I_T(\boldsymbol{z}) = \int K_T(\boldsymbol{z}, \boldsymbol{y}) T(\boldsymbol{y})\, \mathrm{d}\boldsymbol{y}, \tag{B.5}$$

where

$$K_T(\boldsymbol{z}, \boldsymbol{y}) := \int \mathrm{e}^{-\mathrm{i}\nu(|\mathbf{r}_{s,z}|-|\mathbf{r}_{s,y}|)}\, Q(\omega(\nu), s, \boldsymbol{z}) A_P(\omega(\nu), s, \boldsymbol{y})\, \mathrm{d}s \left|\frac{\partial\nu}{\partial\omega}\right| \mathrm{d}\nu. \tag{B.6}$$

In (B.6) we introduce the parameter λ by making the further change of variables $\nu \mapsto \nu' = \nu/\lambda$, obtaining

$$K_T(\boldsymbol{z}, \boldsymbol{y}, \lambda) = \int \mathrm{e}^{-\mathrm{i}\lambda\nu'(|\mathbf{r}_{s,z}|-|\mathbf{r}_{s,y}|)}\, \tilde{A}(\lambda, \nu', s, \boldsymbol{y})\, \mathrm{d}s\, \mathrm{d}\nu', \tag{B.7}$$

where

$$\tilde{A}(\lambda, \nu', s, \boldsymbol{y}) = \lambda^2 A_P(\omega(\lambda\nu'), s, \boldsymbol{y}) Q(\omega(\lambda\nu'), s, \boldsymbol{z}) \left|\frac{\partial\nu'}{\partial\omega}\right|. \tag{B.8}$$

We assume that $\tilde{A}$ satisfies a symbol estimate of the form given in [23]. (Recall that we have assumed that $\omega n_I(\omega) \to$ const as $\omega \to \infty$; this is the case for the Fung–Ulaby model.) Consequently, the stationary phase theorem tells us that the large-λ leading-order contributions to (B.6) come from the critical points satisfying (46) and (47).

Leading-order behavior of (80). To put (80) into the form (B.1), we first make the change of variables $\boldsymbol{\xi} = \lambda\tilde{\boldsymbol{\xi}}$, $\boldsymbol{\xi}' = \lambda\tilde{\boldsymbol{\xi}}'$, where $\lambda = |\boldsymbol{\xi}|$. This change of variables converts the phase to $\phi = \lambda[(\boldsymbol{z} - \boldsymbol{y}) \cdot \tilde{\boldsymbol{\xi}} - (\boldsymbol{z} - \boldsymbol{y}') \cdot \tilde{\boldsymbol{\xi}}']$. The integrand u of (B.2) (with $\boldsymbol{x} \leftrightarrow (\boldsymbol{z}, \tilde{\boldsymbol{\xi}}')$) is then

$$u(\lambda\tilde{\boldsymbol{\xi}}, \lambda\boldsymbol{\xi}', \boldsymbol{y}, \boldsymbol{y}', \boldsymbol{z}) = \frac{1}{\lambda^4}[Q(\lambda\tilde{\boldsymbol{\xi}}, \boldsymbol{z}) A_P(\lambda\tilde{\boldsymbol{\xi}}, \boldsymbol{y}) J(\lambda\tilde{\boldsymbol{\xi}}, \boldsymbol{z}, \boldsymbol{y}) - 1] \times \overline{[Q(\lambda\tilde{\boldsymbol{\xi}}', \boldsymbol{z}) A_P(\lambda\tilde{\boldsymbol{\xi}}', \boldsymbol{y}') J(\lambda\tilde{\boldsymbol{\xi}}', \boldsymbol{z}, \boldsymbol{y}') - 1]}. \tag{B.9}$$

We apply the stationary phase analysis to the $\boldsymbol{z}$ and $\tilde{\boldsymbol{\xi}}'$ integrals, so that N in (B.2) is 4; the leading-order term is (85).

The right-hand side of (B.2) decays more rapidly than λ^{-2} provided u satisfies a symbol estimate as in [23]. This is the case because (a) the flight path is smooth, (b) for the operating frequencies of the radar, the permittivity ϵ_r is smooth and (c) P is assumed to satisfy symbol estimates. Although derivatives with respect to $\tilde{\boldsymbol{\xi}}'$ give rise to factors of λ, because u involves P, whose derivatives decay increasingly rapidly in ω (ω being proportional to $|\boldsymbol{\xi}| = \lambda$), these extra factors of λ do not lead to an overall worsening of the decay rate in λ. For the calculation of (85), we assume that Q is smooth; then smoothness of (94) can be checked, so that the assumption is consistent with the result.

Appendix C. Beylkin determinant

In order to compute the Jacobian determinant for the Stolt change of variables, we start from equations (15), (34) and (51):

$$\boldsymbol{\Psi}(x_1, x_2) = [x_1, x_2, \psi(x_1, x_2)]^{\mathrm{T}}, \tag{C.1}$$

$$\mathbf{r}_{s,\boldsymbol{x}} = \boldsymbol{\Psi}(x_1, x_2) - \boldsymbol{\gamma}(s), \tag{C.2}$$

$$|\mathbf{r}_{s,\boldsymbol{x}}| = \sqrt{[\gamma_1(s) - x_1]^2 + [\gamma_2(s) - x_2]^2 + [\gamma_3(s) - \psi(\boldsymbol{x})]^2}, \tag{C.3}$$

$$\nabla_{\boldsymbol{x}} |\mathbf{r}_{s,\boldsymbol{x}}| = -\frac{1}{|\mathbf{r}_{s,\boldsymbol{x}}|} \begin{bmatrix} \gamma_1(s) - x_1 + (\gamma_3(s) - \psi(\boldsymbol{x})) \frac{\partial \psi}{\partial x_1} \\ \gamma_2(s) - x_2 + (\gamma_3(s) - \psi(\boldsymbol{x})) \frac{\partial \psi}{\partial x_2} \end{bmatrix}. \tag{C.4}$$

Therefore, for $\boldsymbol{z} = \boldsymbol{y}$ in equation (51), and for flat topography ($\psi = 0$),

$$-\Xi(\omega, s, \boldsymbol{z}, \boldsymbol{z}) = \frac{2\omega n_R(\omega)}{c_0 |\mathbf{r}^0_{s,z}|} \begin{bmatrix} \gamma_1(s) - z_1 \\ \gamma_2(s) - z_2 \end{bmatrix}, \tag{C.5}$$

where $\mathbf{r}^0_{s,z} = \boldsymbol{\gamma}(s) - [z_1, z_2, 0]$. Furthermore, for $\boldsymbol{y} = \boldsymbol{z}$, the (absolute value of the) Jacobian determinant is the reciprocal of

$$\left| \frac{\partial \boldsymbol{\xi}}{\partial(\omega, s)} \right| = \left| \det \begin{bmatrix} \frac{\partial \xi_1}{\partial \omega} & \frac{\partial \xi_1}{\partial s} \\ \frac{\partial \xi_2}{\partial \omega} & \frac{\partial \xi_2}{\partial s} \end{bmatrix} \right|. \tag{C.6}$$

Now, we introduce the frequency-dependent functions

$$v_p(\omega) = \frac{c_0}{n_R(\omega)}, \tag{C.7}$$

$$v_g(\omega) = \frac{c_0}{n_R(\omega) + \omega \partial_\omega n_R(\omega)}, \tag{C.8}$$

where $\partial_\omega := \frac{\partial}{\partial \omega}$. Then, a straightforward calculation shows that

$$\frac{\partial \xi_1}{\partial s} = \frac{2\omega}{v_p(\omega)} P_\perp \dot{\boldsymbol{\gamma}}(s) \cdot \frac{\partial \boldsymbol{\Psi}}{\partial z_1}, \qquad \frac{\partial \xi_2}{\partial s} = \frac{2\omega}{v_p(\omega)} P_\perp \dot{\boldsymbol{\gamma}}(s) \cdot \frac{\partial \boldsymbol{\Psi}}{\partial z_2}, \tag{C.9}$$

where $P_\perp \dot{\gamma}(s)$ denotes the scaled projection of $\dot{\gamma}(s)$ onto the plane perpendicular to $\widehat{\mathbf{r}^0_{s,z}}$:

$$P_\perp \dot{\gamma}(s) := \frac{\dot{\gamma}(s) - \widehat{\mathbf{r}^0_{s,z}}(\widehat{\mathbf{r}^0_{s,z}} \cdot \dot{\gamma}(s))}{|\mathbf{r}^0_{s,z}|}. \tag{C.10}$$

We furthermore obtain

$$\frac{\partial \xi_1}{\partial \omega} = \frac{2}{v_g(\omega)} \widehat{\mathbf{r}^0_{s,z}} \cdot \frac{\partial \boldsymbol{\Psi}}{\partial z_1}, \qquad \frac{\partial \xi_2}{\partial \omega} = \frac{2}{v_g(\omega)} \widehat{\mathbf{r}^0_{s,z}} \cdot \frac{\partial \boldsymbol{\Psi}}{\partial z_2}. \tag{C.11}$$

Inserting (C.9)–(C.11) into (C.6), we arrive at the reciprocal of the Jacobian determinant, $J(s, \omega, \boldsymbol{z}, \boldsymbol{z})$, as

$$\frac{1}{J} = \left| \frac{4\omega}{v_p(\omega) v_g(\omega)} \det \begin{bmatrix} \widehat{\mathbf{r}^0_{s,z}} \cdot \partial_{z_1} \boldsymbol{\Psi} & P_\perp \dot{\gamma}(s) \cdot \partial_{z_1} \boldsymbol{\Psi} \\ \widehat{\mathbf{r}^0_{s,z}} \cdot \partial_{z_2} \boldsymbol{\Psi} & P_\perp \dot{\gamma}(s) \cdot \partial_{z_2} \boldsymbol{\Psi} \end{bmatrix} \right|. \tag{C.12}$$

Comparing (C.12) to the result presented in [13], we note the multiplicative factor $4\omega/(v_p(\omega)v_g(\omega))$ which is needed here to account for the dispersivity.

As a concrete example, if we consider a circular trajectory with radius R, centered at the origin, and at a height h above a flat topography, we have

$$\Xi(s, \omega, 0, 0) = \frac{-2\omega n_R(\omega) R}{c_0 \sqrt{R^2 + h^2}} \begin{bmatrix} \cos(s) \\ \sin(s) \end{bmatrix}, \tag{C.13}$$

where the trajectory has been parametrized such that $0 \leqslant s < 2\pi$. This implies that the reciprocal of the Beylkin determinant at the origin is

$$\left| \frac{\partial \boldsymbol{\xi}}{\partial(\omega, s)} \right| = \frac{4\omega}{c_0^2} n_R(\omega) \left(n_R(\omega) + \omega \partial_\omega n_R(\omega) \right) \frac{R}{R^2 + h^2}. \tag{C.14}$$

References

[1] Brillouin L 1960 *Wave Propagation and Group Velocity* (New York: Academic)

[2] Cheney M and Nolan C J 2004 Synthetic-aperture imaging through a dispersive layer *Inverse Problems* **20** 507–32

[3] Morales J H 2008 Synthetic-aperture radar imaging and waveform design for dispersive media *PhD Thesis* Department of Mathematical Sciences, Rensselaer Polytechnic Institute, Troy, NY, USA

[4] Kristensson G 1991 *Direct and Inverse Scattering Problems in Dispersive Media–Green's Functions and Invariant Imbedding Techniques (Methoden und Verfahren der Mathematischen Physik.* vol 37*)* (Frankfurt am Main, Germany: Peter Lang)

[5] Beezley R S and Kruger R J 1985 An electromagnetic inverse problem for dispersive media *J. Math. Phys.* **26** 317–25

[6] Budko N V 2002 Linearized electromagnetic inversion of inhomogeneous media with dispersion *Inverse Problems* **18** 1509–23

[7] Fuks P, Karlsson A and Larson G 1994 Direct and inverse scattering from dispersive media *Inverse Problems* **10** 555–71

[8] Oughstun K E and Sherman G C 1994 *Electromagnetic Pulse Propagation in Causal Dielectrics* (Berlin: Springer)

[9] Bui D D 1995 On the well posedness of the inverse electromagnetic scattering problem for a dispersive medium *Inverse Problems* **11** 835–63

[10] He S and Weston V H 1997 Three-dimensional electromagnetic inverse scattering for bi-isotropic dispersive media *J. Math. Phys.* **38** 182–95

[11] Gustafsson M 2000 Wave splitting in direct and inverse scattering problems *PhD Thesis* Department of Applied Electronics, Electromagnetic Theory, Lund University, Lund, Sweden

[12] Tsynkov S V 2009 On SAR imaging through the earth ionosphere *SIAM J. Imaging Sci.* **2** 140–82

[13] Nolan C J and Cheney M 2003 Synthetic aperture inversion of arbitrary flight paths and non-flat topography *IEEE Trans. Image Process.* **12** 1035–43

[14] Nolan C J and Cheney M 2002 Synthetic aperture inversion *Inverse Problems* **18** 221–36

[15] Yazıcı B, Cheney M and Yarman C E 2006 Synthetic aperture inversion for an arbitrary flight trajectory in the presence of noise and clutter *Inverse Problems* **22** 1705–29
[16] Varslot T, Yarman C E, Cheney M and Yazıcı B 2007 A variational approach to waveform design for synthetic-aperture imaging *Inverse Problems and Imaging* **1** 577–92
[17] Jackson J D 1999 *Classical Electrodynamics* 3rd edn (New York: Wiley)
[18] Sihvola A 1999 *Electromagnetic Mixing Formulas and Applications* (London, UK: The Institution of Electrical Engineers)
[19] Milonni P W 2005 *Fast Light, Slow Light and Left-Handed Light (Series in Optics and Optoelectronics)* (Bristol, UK: Institute of Physics)
[20] Cheney M and Borden B 2009 Problems in synthetic-aperture radar imaging *Inverse Problems* **25** 123005
[21] Cheney M 2001 A mathematical tutorial on synthetic aperture radar *SIAM Rev.* **43** 301–12
[22] Evans G, Blackedge J and Yardley P 2001 *Analytic Methods for Partial Differential Equations* (London, UK: Springer)
[23] Grigis A and Sjöstrand J 1994 *Microlocal Analysis for Differential Operators (London Mathematical Society—Lecture Note Series* vol 196*)* (Cambridge: Cambridge University Press)
[24] Born M and Wolf E 1993 *Principles of Optics* 6th edn (Oxford: Pergamon)
[25] Scharf L L 1991 *Statistical Signal Processing: Detection, Estimation, and Time Series Analysis* (New York: Addison-Wesley)
[26] Jenkins G M and Watts D G 1968 *Spectral Analysis and its Applications* (San Francisco: Holden Day)
[27] Stein M 1999 *Interpolation of Spatial Data* (New York: Springer)
[28] Blahut R E 2004 *Theory of Remote Image Formation* (Cambridge, UK: Cambridge University Press)
[29] Dhawan A P 2003 *Medical Image Analysis (IEEE Press Series in Biomedical Engineering)* (New York: Wiley Interscience)
[30] Fung A K and Ulaby F T 1978 A scatter model for leafy vegetation *IEEE Trans. Geosci. Electron.* **16** 281–6
[31] Albanese R, Penn J and Medina R 1989 Short-rise-time microwave pulse propagation through dispersive biological media *J. Opt. Soc. Am.* A **6** 1441–6
[32] Oughstun K E 2005 Dynamical evolution of the Brillouin precursor in Rocard–Powles–Debye model dielectrics *IEEE Trans. Antennas Propag.* **53** 1582–90
[33] Cartwright N A and Oughstun K E 2007 Uniform asymptotics applied to ultrawideband pulse propagation *SIAM Rev.* **49** 628–48
[34] El-Rayes M A and Ulaby F T 1987 Microwave dielectric spectrum of vegetation-part: I. Experimental observations *IEEE Trans. Geosci. Remote Sens.* **25** 541–9
[35] Ulaby F T and El-Rayes M A 1987 Microwave dielectric spectrum of vegetation: part II. Dual-dispersion model *IEEE Trans. Geosci. Remote Sens.* **25** 550–7